OF
AD
A063218

END
DATE
FILMEQ

3-79

DDC

UNDERWATER SYSTEMS INC.

AD A063218
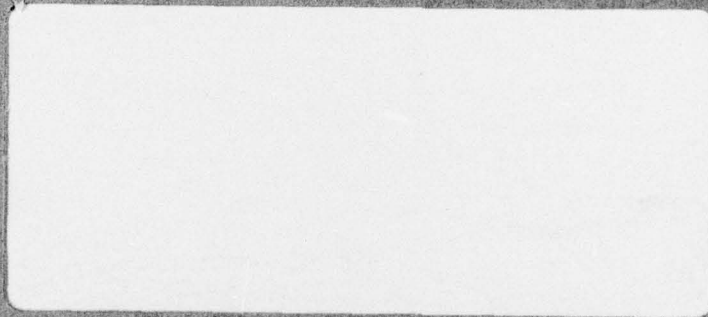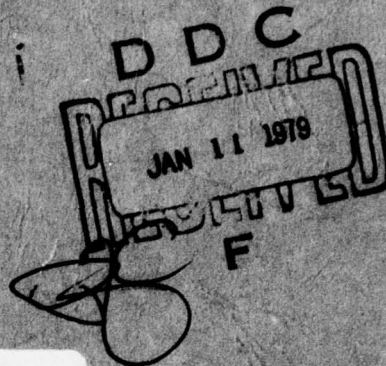
LEVEL

DDC
JAN 11 1979
F

79 01 10 059

Final Report
Task II

D D C

JAN 11 1979

F
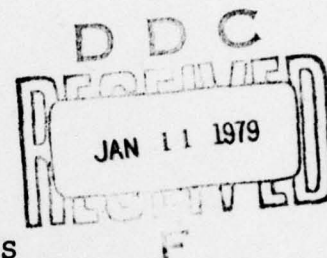
INVESTIGATION OF THE POTENTIALITIES
OF USING SEISMIC SENSORS FOR THE
DETECTION OF SHIPS AND OTHER
NAVAL PLATFORMS

September 24, 1978

By:
Richard J. Hecht

With Contributions By:
Curtis I. Holmer
Louis A. Mole

Contract N00014-74-C-0294
Task No. 089-104

Submitted To:

Office of Naval Research
Code 465
Department of the Navy
Arlington, VA   22217

UNDERWATER
SYSTEMS, Inc.

79 01 10 059

World Building • 8101 Georgia Ave. • Silver Spring, Md. 20910 • (301) 589-1188

REPORT DOCUMENTATION PAGE		READ INSTRUCTIONS BEFORE COMPLETING FORM
1. REPORT NUMBER	2. GOVT ACCESSION NO.	3. RECIPIENT'S CATALOG NUMBER
4. TITLE (and Subtitle) Investigation of the Potentialities of Using Seismic Sensors for the Detection of Ships and Other Naval Platforms		5. TYPE OF REPORT & PERIOD COVERED Final Report
		6. PERFORMING ORG. REPORT NUMBER
7. AUTHOR(s) Richard J. Hecht Curtis I. Holmer Louis A. Mole		8. CONTRACT OR GRANT NUMBER(s) N00014-74-C-0294
9. PERFORMING ORGANIZATION NAME AND ADDRESS Underwater Systems, Inc. 8121 Georgia Ave. Silver Spring, MD 20910		10. PROGRAM ELEMENT, PROJECT, TASK AREA & WORK UNIT NUMBERS NR 089-104
11. CONTROLLING OFFICE NAME AND ADDRESS Office of Naval Research (Code 465) Department of the Navy Arlington, VA 22217		12. REPORT DATE 24 September 1978
		13. NUMBER OF PAGES 90
14. MONITORING AGENCY NAME & ADDRESS(If different from Controlling Office)		15. SECURITY CLASS. (of this report) UNCLASSIFIED
		15a. DECLASSIFICATION/DOWNGRADING SCHEDULE

16. DISTRIBUTION STATEMENT (of this Report)

Approved for public release; distribution unlimited

17. DISTRIBUTION STATEMENT (of the abstract entered in Block 20, if different from Report)

18. SUPPLEMENTARY NOTES

19. KEY WORDS (Continue on reverse side if necessary and identify by block number)

seismic detection, seismic propagation, shallow water propagation, geophones, hydrophones, attenuation, arrays background noise, signal to noise.

20. ABSTRACT (Continue on reverse side if necessary and identify by block number)

(U) The potential of using geophones and seismic paths for the acoustic detection of ships is investigated using available data and theory. The use of seismic paths offer the potential of a reliable detection range that is independent of the sound velocity profile in the water. An estimate of the achievable reliable range using a multiaxial geophone is 10 to 20 km. The attenuation of sound in the sediment is the controlling factor in signal propagation. The estimates need to be confirmed by experimental investigation.

DD FORM 1473 EDITION OF 1 NOV 65 IS OBSOLETE
1 JAN 73

356 270

i

TABLE OF CONTENTS

iii

LIST OF FIGURES

LIST OF TABLES

EXECUTIVE SUMMARY

The conditions under which seismic sensors offer opportunities
for the detection of acoustic targets in shallow water in the
1 to 30 Hz frequency region were examined using existing theo-
retical and experimental knowledge. Six aspects of the problem
were examined:

1.   environmental geometry

2.   the physical environment

3.   background noise

4.   the geophone as a sensor

5.   seismic array design

6.   measurements needed to improve knowledge

Because of the much higher attenuation in the bottom than
in the water, sound transmission in the water is superior to
that in the bottom when favorable sound velocity profiles are
present in the water. However, when negative sound velocity
gradients exist in the water, propagation through the bottom
offers the potential of a reliable propagation path that is
unaffected by the velocity gradient in the water. Thus,
seismic sensors offer a minimum range of detection. A 10 to
20 km reliable range is estimated for seismic detection for
average bottom conditions. Insufficient experimental data exist
to confirm this estimate; hence, several critical experiments
have been recommended.

1

Two issues arise in understanding, predicting, and sensing acoustic signals propagating in the bottom. These two are:

1. What is the best method to map the bottom?
2. What is the optimum way to sample the propagating energy?

An analysis of the geophone as a reciever shows that its inherent construction offers a 4.8 dB gain over an omnidirectional hydrophone in an isotropic noise field.

A theoretical development was performed that shows a horizontal geophone is superior to a vertical one for P-wave energy for ratios of phase velocities to compressional velocity of less than the $\sqrt{2}$.

Three short range data sets were found that show that the signal to noise ratio (SNR) for horizontal geophones is larger than that for hydrophones located nearby.

Quantitative data obtained using geophones is scarce and data that compares the performance of geophones to hydrophones is even more limited.

The attenuation of sound in the bottom will chiefly determine the range to which sound will propagate through the bottom and yet have a useful amplitude.

1. INTRODUCTION

This is the final report of a study conducted in accordance with Task II of ONR Contract No. N00014-74-C-0294. The purpose of this study was to identify conditions under which seismic sensors offer opportunities for detection of acoustic targets in shallow water, based upon existing theoretical and experimental knowledge. Both signal transmission and noise were considered in an effort to determine whether sensors should be embedded in the sea floor, be located in the shallow water environment, at some distance in deep water, or on land.

In this study, seismic detection was defined as the detection of a signal in which a significant part of the transmission path is through the ocean bottom. Six aspects of seismic detection were investigated:

1. environmental geometry

2. the shallow water environment

3. background noise

4. the geophone as a detector

5. seismic array design

6. measurements needed to improve the state of knowledge.

These are each discussed in Section 2. Section 3 discusses
outstanding seismic detection issues that prevent a definitive
resolution of all the problems investigated and outlines a
program for gathering needed information. Section 4 contains
a short summary. Mathematical derivations of discrete prop-
erties of the acoustic sound field are included in the Appendices.

2. SEISMIC DETECTION CONSIDERATIONS

2.1 Environmental Geometry

A generalized description of the propagation medium, or the communication channel, together with representative locations of an acoustic source and receivers are illustrated in Figure 1. The transmission medium and communications channel analogy is intuitively appealing since both exhibit the equivalent characteristics of a non-linear, memory-less information channel. The sources (targets) of interest are characterized by (1) a spectrum level of 160 to 180 dB//μPa, (2) a 1 to 30 Hz frequency range, (3) a source depth in water of 0 to 400 meters, and (4) a spectrum characterized by tonals. The typical locations for receivers that may be used to receive seismic energy are in the bottom, in the water, or in boreholes. R_1 and R_4 in Figure 1 are located in the water and depend on bottom-propagated energy to be refracted into the water for reception. R_2 and R_3 are located at shallow depths in the bottom. Paths to these receivers can be propagated either through a bottom layer or from the waterborne energy near the water-bottom interface. R_5 and R_6 are located in a borehole. R_5 is located in the sediment and R_6 in the crystalline basement. These two receivers are placed so as to receive energy propagating in the layer in which they are located. Since the source (target) is always located in the water portion of the communication channel, the total capability of this time-variable heterogeneous channel needs to be considered. The receivers should be positioned to optimally sample the channel to obtain

5
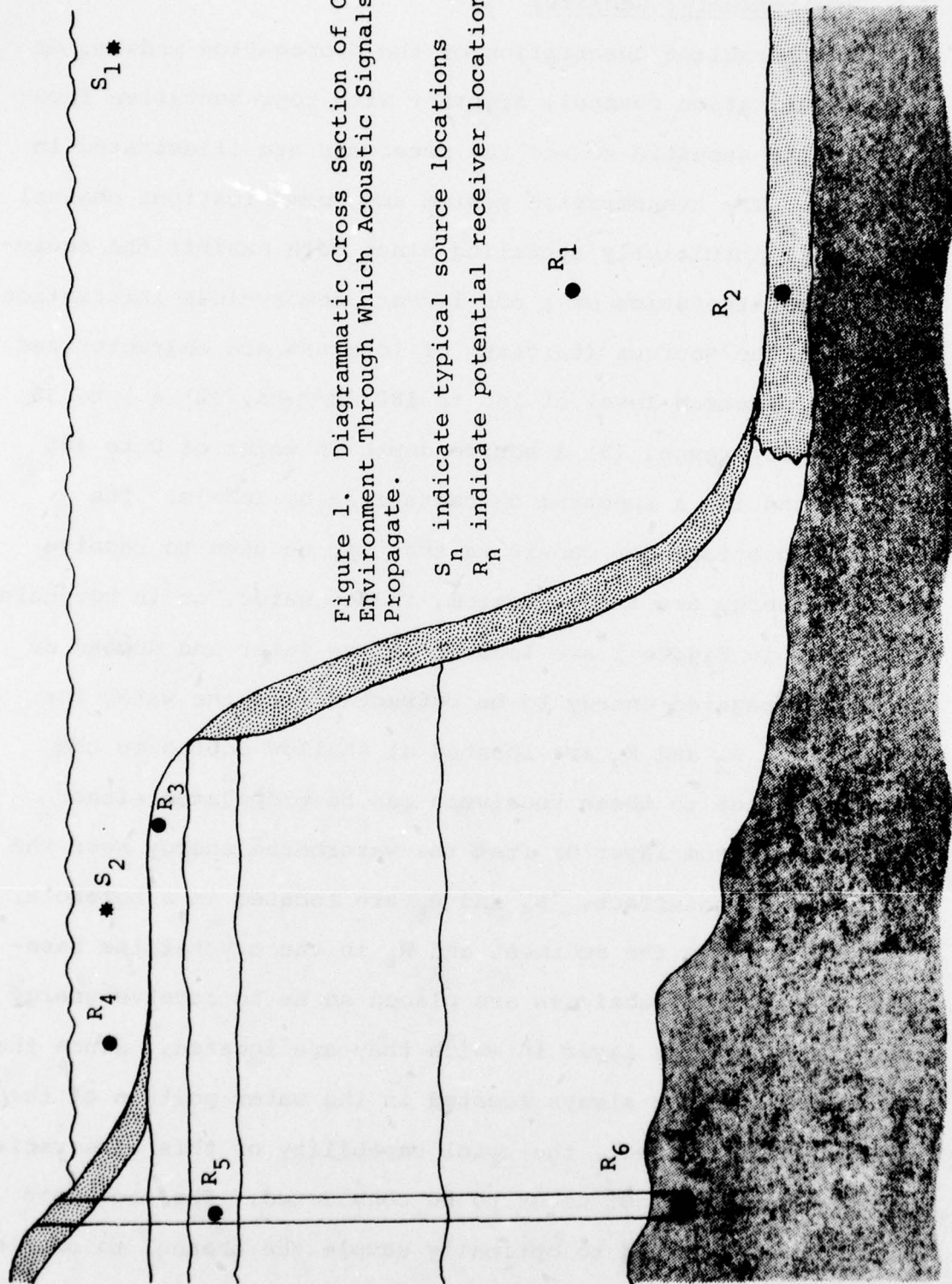
Figure 1. Diagrammatic Cross Section of Oceanic Environment Through Which Acoustic Signals Propagate.

S_n indicate typical source locations
R_n indicate potential receiver locations

the best signal to noise ratio.

When favorable velocity profiles exist in the water, transmission of energy through the water is superior to transmission through the bottom. When the velocity profile in the water is unfavorable, propagation through the bottom (seismic detection) offers a potential of reliable propagation that is essentially unaffected by propagation conditions in the water. By combining the capabilities of water and bottom propagation, the communication channel can guarantee a minimum range of detection via predominantly seismic paths and yet retain the added capability of the paths that are predominantly waterborne.

The communication channel, as discussed, exists in both shallow and deep water. However, it is in shallow water that it appears that the largest gain in signal propagation can be achieved by pursuing the total communication channel concept.

2.2 Shallow Water Environment

Shallow water investigations that recognized the interaction of the water and bottom were begun prior to World War II. Probably the best known participants in these investigations were Ewing, Pekeris, Press and Worzel of Columbia University. Their work was summarized and interpreted after the War in Geological Society of America Memoir 27 (Reference 1), which even today is the baseline reference for shallow water propagation. Three applicable results from the Memoir are the interpretation of sound transmission; the Ewing effect, which is the dispersion observed in the lower frequency region; and the

7

concept of depth of penetration of acoustic energy into the bottom.

The guided transmission theory for shallow water was adapted from electromagnetic theory. Of particular importance is the description of the pressure and particle velocity as a function of depth. The vertical distribution of pressure in the water has been confirmed by Ferris (Reference 2) and others. Figure 2 is a typical amplitude distribution versus depth for the first mode at a frequency slightly above cut-off, for typical low density and low velocity ratios for a liquid bottom. Of particular interest is the pressure amplitude near the bottom. For this particular case, the receiver location for the best signal strength is near the sediment-water interface.

The depth of penetration was defined by Pekeris (Reference 1) as the depth at which no further information on the structure of the bottom at greater depths can be obtained from dispersion data. As a quantitative measure, he used the section of the bottom that contained 99% of the total energy in the bottom. Another way to look at depth of penetration is that all useful guided energy will be above that depth. Since we are interested in locating potential seismic energy paths, the depth of penetration tells us how deep we have to consider the sediments or rock. Attenuation in the sediments may also limit the depths that need to be considered. The concept of penetration depth was extended by Williams (Reference 3) in his concept of hidden depths.

The penetration depth for a given set of environmental

Water 600 ft Density = ρ_1
Velocity = c_1

Bottom 750 Density = ρ_2
Velocity = c_2

Source Depth - 300 ft

Frequency - 12 Hz

ρ_1 - 1.0

ρ_2 - 1.1

C_1 - 4800

C_2 - 4900

Total Depth = 6639 ft

1500

2250

3000

3750

4500

5250

6000
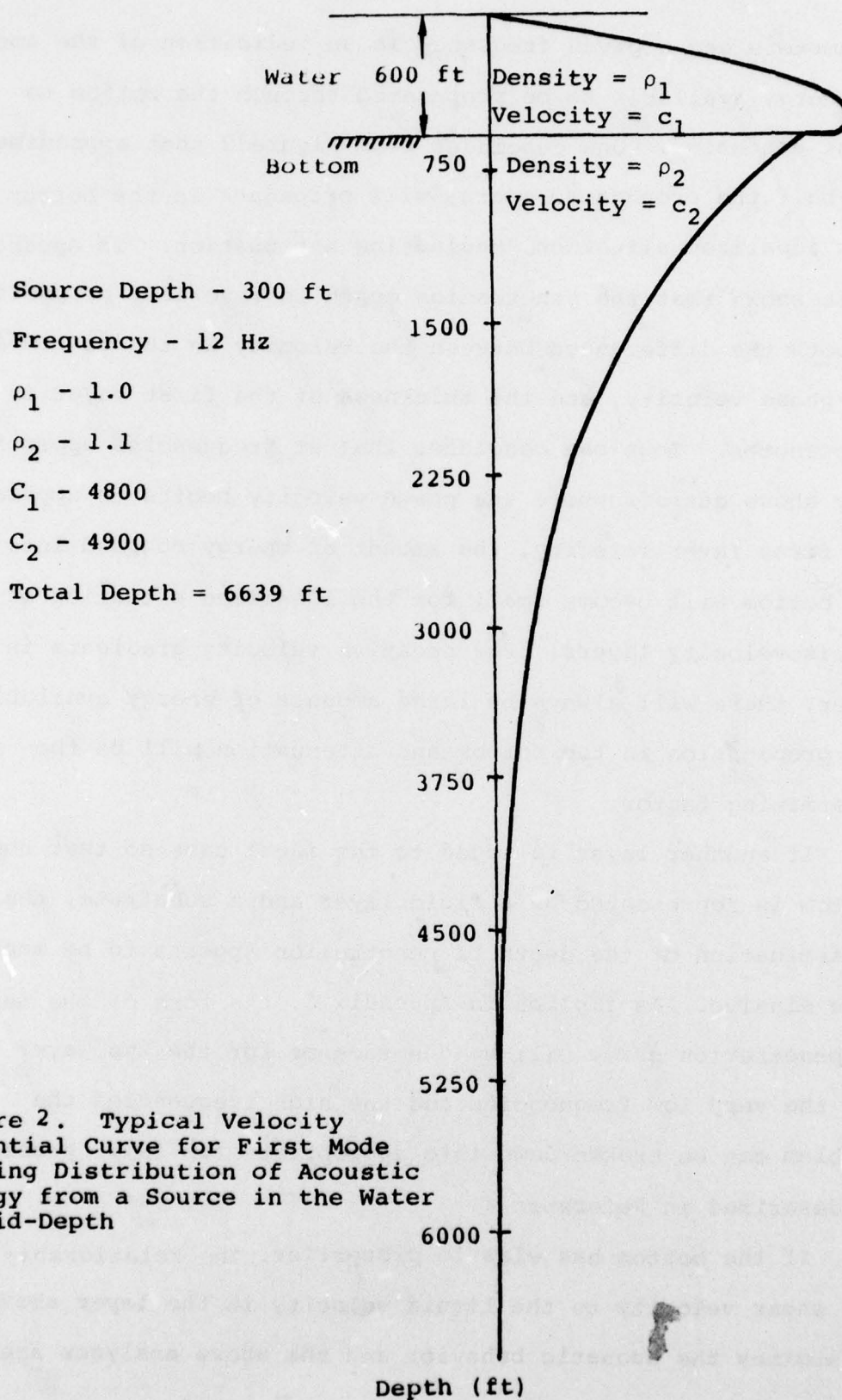
Figure 2. Typical Velocity
Potential Curve for First Mode
Showing Distribution of Acoustic
Energy from a Source in the Water
at Mid-Depth

Depth (ft)

9

parameters and a given frequency is an indication of the amount of energy available to be propagated through the bottom to large distances. One concludes from Figure 2 that approximately one-half the propagated energy will propagate in the bottom for this idealized situation, neglecting attenuation. In Appendix A it is shown that the penetration depth is inversely proportional to both the differences between the velocity in the bottom and the phase velocity, and the thickness of the first layer in wavelengths. Thus one concludes that at frequencies appreciably above cut-off where the phase velocity begins to approach the first layer velocity, the amount of energy coupled into the bottom will become small for the idealized situation of two isovelocity layers. For negative velocity gradients in the water, there will always be large amounts of energy available for propagation in the bottom and attenuation will be the determining factor.

If another layer is added to the ideal case so that the bottom is represented by a fluid layer and a substrate, the determination of the depth of penetration appears to be much more elusive. As implied in Appendix C, the form of the depth of penetration curve will be the same as for the two layer case. For the very low frequencies and the high frequencies the problem can be broken down into appropriate two layer problems as described in Reference 4.

If the bottom has elastic properties, the relationship of the shear velocity to the liquid velocity in the layer above determines the acoustic behavior and the above analyses are

10

indicative. When the shear velocity is lower that the overlying liquid velocity, the situation appears to present a dichotomy. On the one hand, theory shows that guided transmission is at best minimal, while on the other hand experimental data from shallow water experiments show that guided transmission is possible with varying amounts of attenuation. This dichotomy may arise from a lack of environmental data.

The phenomenon of dispersion in the water wave was discovered by Ewing (Reference 1). Observed dispersion is related to the depth, density, and velocity ratios of the transmission media. Pekeris makes the point that if the dispersion curves from different paths are indistinguishable, so are the parameters of the media. From this statement one would further conclude that the measurement of dispersion is a pragmatic way of describing the acoustic behavior of the ocean bottom.

In 1955 Kornhauser and Raney (Reference 5) added the effect of attenuation in the bottom to the wave description of propagation as a function of frequency and mode number, but the attenuation coefficients were not specified.

The next significant step in understanding shallow water propagation as well as propagation through the bottom was made by Tolstoy, Clay and Blaik (References 4 and 6). In their Fire Island experiment it was concluded that bottom parameters determined by seismic refraction were inferior to acoustic-determined parameters (Reference 7). The experiment showed the adequacy of the wave model to predict short range shallow water propagation.

11

In Figure 3 relative propagation loss contours for a 10 and
a 14 Hz source are shown (after Reference 6). The receiver
is a vertical geophone located in a borehole on the beach at
a depth of 119 meters. The indicated propagation loss is greater
than would occur in spherical spreading (20 log R). This result
will be discussed further in a following section.

The effect of a mixture or a loaded liquid has been dis-
cussed by Officer (Reference 8). For the water-bottom interface
Figure 4a shows the resulting velocity of the upper region of
a structureless bottom to be less than that of the water. Under
such a condition the natural question to ask is, where is the
water-bottom interface for guided transmission? The above
results assume an ideal situation. If a water-filled sediment
is considered, then the sediment will exhibit some structure;
probably very little at the water-bottom interface, but
increasing with depth. Also water has viscosity. With
these added real life parameters, consider a high porosity
sediment. The viscosity of the water will cause a sediment
velocity that is dependent on frequency as illustrated in Figure 4b.
A medium that exhibits such behavior will be highly dispersive.
The mixture effects are undoubtedly present in the first bottom
layer and need to be considered as well as the structure in
the sediment.

In an experiment using a Texas Tower as a receiving station,
Barakos studied shallow water propagation as a function of season
(Reference 9). Ranges in excess of 100 nautical miles were

12
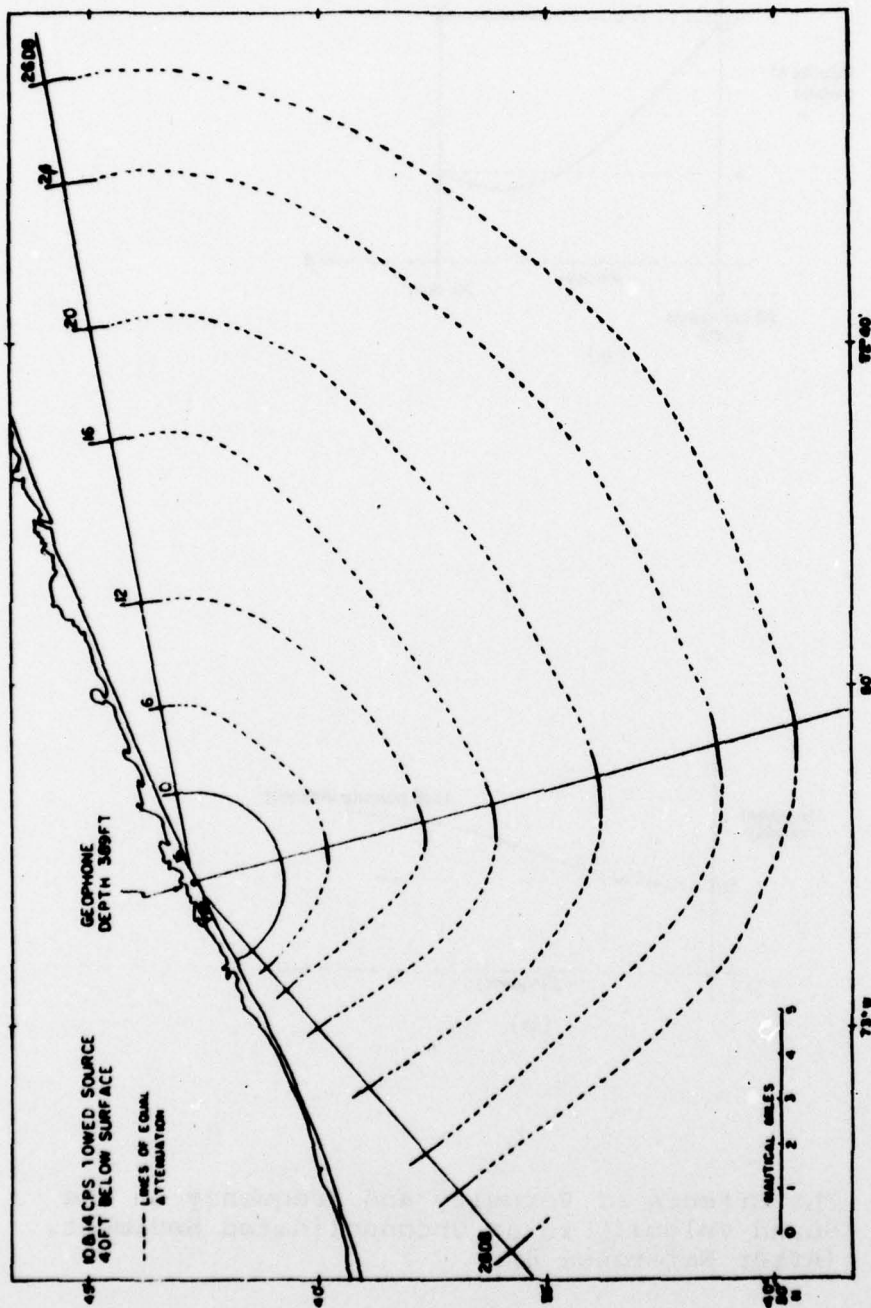
Figure 3. Average Attenuation of the Vertical Component of Particle Velocity as a Function of Range and Direction for Low Frequency Sound.

The detector depth is 389 ft. The water increases in depth perpendicular to the shore, and the depth to basement increases in the 170° direction. Attenuation is given for each of the runs (represented by radial lines) in dB relative to the amplitude at 2 miles. (After Reference 6).
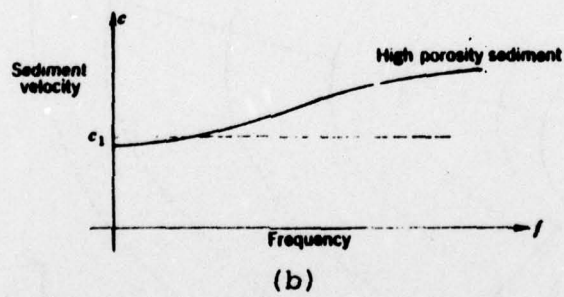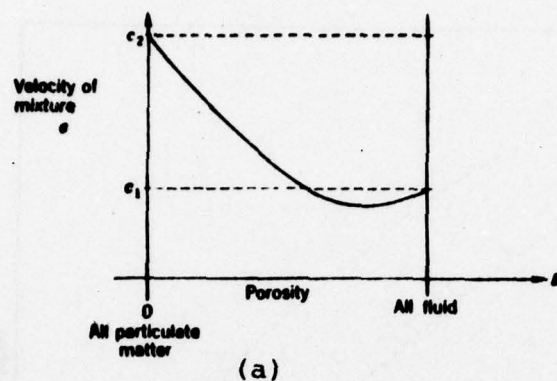
Figure 4. The Effects of Porosity and Frequency on the Sound Velocity in an Unconsolidated Sediment. (After Reference 8).

14

achieved using bomb shots as sources with favorable sound velocity profiles in the water. By using the dispersion concept of Ewing (Reference 1), Barakos acoustically categorized a large area of the continental shelf between New Jersey and Nantucket. Bucker added to the dispersion concept by advancing the idea of measuring attenuation by quantitatively measuring the amplitude in small frequency increments for each mode (Reference 10).

To categorize the shelf, Houtz and others (Reference 11) developed a method for measuring interval velocities of the sediments on the shelf using sonobuoys. Interface waves, in contrast to body waves, are a possible way to obtain acoustic information transmission over long distances. This possibility is an extension of teleseismic observations at low frequencies through the 3 to 30 Hz region of interest. Two interfaces are of special interest, the water-bottom, and the sedimentary rock-crystalline basement interfaces.

Theoretically there are no limitations in the generation of interface waves at a liquid-solid interface. McLeroy (Reference 12) observed an interface wave during his sea bottom elastic wave experiments. Although the wave did not seem to fit exactly any of the theoretical surface waves, it was interpreted as a Stoneley wave. The wave consisted mainly of energy in the frequency range of 6 to 7 Hz, a frequency well below cutoff for guided propagation. Propagation loss as a function of range indicates that the Stoneley wave has 3 dB less loss between the ranges of 100 and 2000 ft than does the waterborne energy.

15

Hence, the observed interface wave may be a viable path for distinct frequencies (in this case 6-7 Hz).

In another experiment Bucker, et al. (Reference 13) used Stonely waves to measure the shear velocity in the bottom. The propagating signal was essentially sinusoidal at 20 and 25 Hz for each of two cases. The extent of the range measurement was very limited, only 47 ft. The propagation loss was considered to consist of a cylindrical spreading loss and an attenuation factor of 0.06 and 0.1 dB/ft for each of two cases. If the attenuation factor is extended linearly with range to 10 km the loss would be over 3000 dB. Either the propagation is very poor or short range measurements cannot be extended to longer ranges. In any case more experimental data is needed on surface wave propagation at the water-bottom interface. No information was found about a source in shallow water generating interface waves between the various rock layers.

In all the shallow water propagation studies of the past, one theme is highlighted - an adequate acoustic description of the bottom is needed. Tolstoy (Reference 7), through a sensitivity analysis, showed the importance of accurately knowing the acoustic impedance and layer thickness. An adequate description of the bottom is one of the prerequisites for being able to predict acoustic propagation in the bottom with confidence and accuracy. Another bottom parameter that has a controlling effect on propagation is attenuation.

16

Attenuation in the sediments has been of concern since the early 1950s. Tolstoy developed empirical attenuation coefficients based on his Fire Island data following the method of Kornhauser and Raney (Reference 5). Nominal values for the exponential decay were 5.0×10^{-4}/m at 10 and 14 Hz (Reference 4). Hamilton and others began measuring attenuation and relating it to the porosity of sediments. In a recent study (Reference 14) he summarized the attenuation of both compressional and shear waves; the results are shown in Table 1. Attenuation is in terms of a logarithmic decrement per wavelength (Δ), which is the natural log of the ratio of the amplitude of a wave at successive maxima. Therefore attenuation (α) as a function of range can be described as $\alpha(R) = e^{-\Delta R / \lambda}$, where R is range and λ is wavelength. For compressional waves, sand and fine sand appear to compose one attenuation group and the silt clays and clayey silts another. The difference in attenuation between these two groupings is a factor of six. Figure 5 shows attenuation versus range for three values of logarithmic decrement, 0.1, 0.017 and 0.005, for a frequency of 3 Hz and a wavelength of 600 m. The graph dramatically shows the high attenuation expected for a logarithmic decrement of 0.1, which is representative of sand. The curve for a decrement of 0.005 is representative of crystalline rocks.

Since there are no known long range measurements of propagation through these types of sediments, some conjectures will be made as to what one might expect from a source in the water. A simple propagation loss (PL) equation will be defined:

Table 1

LOGARITHMIC DECREMENTS OF
ACOUSTIC ENERGY IN SEDIMENTS

| | Compressional Waves | | | Sheer Waves |
	Low	High	Average	Average
Sand	0.073	0.130	0.100	0.3
Fine Sand	–	–	0.103	–
Silt Clays	0.007	0.028	0.017	0.1
Clayey Silt	–	–	0.016	–

18
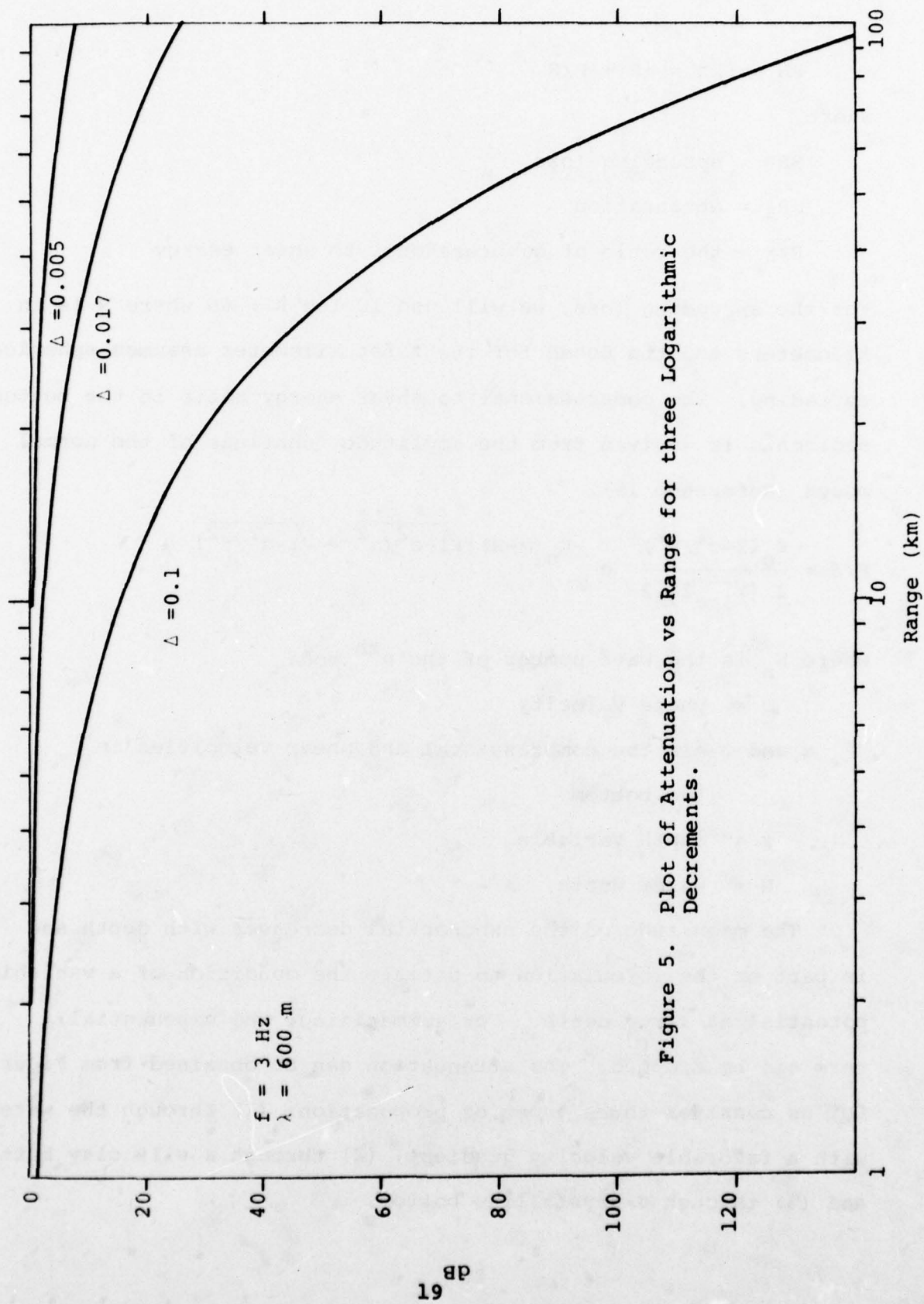
Figure 5. Plot of Attenuation vs Range for three Logarithmic Decrements.

$\Delta = 0.005$

$\Delta = 0.017$

$\Delta = 0.1$

$f = 3$ Hz
$\lambda = 600$ m

Range (km)

dB

19

$$PL = SRL = \alpha R + P/S$$

where

SLR = spreading loss

αR = attenuation

P/S = the ratio of compressional to shear energy

For the spreading loss, we will use 10 log R + 60 where R is in kilometers and the 60 dB for the first kilometer assumes spherical spreading. The compressional to shear energy ratio in the bottom sediments is derived from the amplitude functions of the normal modes (Reference 15).

$$P/S = \frac{K_n(2-c^2/\beta^2)}{2\,(\sqrt{1-c^2/\alpha^2}}\ \ e^{\ -K_n(z-H)\,[\sqrt{1-c^2/\alpha^2}\ -\ \sqrt{1-c^2/\beta^2}\,]}$$

where K_n is the wave number of the nth mode

c = phase velocity

α and β are the compressional and shear velocities in

the bottom

z = depth variable

H = water depth

The magnitude of the exponential decreases with depth and is part of the formulation to satisfy the condition of a vanishing potential at large depth. For summarizing, the exponential term can be dropped. The attenuation can be obtained from Figure 5. Let us consider three types of propagation: (1) through the water with a favorable velocity gradient, (2) through a silt clay bottom and (3) through a crystalline bottom.

20

For frequencies well above cut-off we would expect the following at a 10 km range.

	Type	SLR	αR	P/S	Total PL	Signal Level	Received Signal Level
Water Path	P	80	≃6	0	86	160	74
Silt Clay Path	P	80	23	*	103	160	57
Crystalline Path	S	80	22	1	103	160	57

*Unknown

The above tabulation is probably optimistic but represents the types of differences for different paths through the communication channel. The water path is primarily controlled by the water velocity gradient, and the boundaries. When the velocity gradient becomes negative the water path is strongly attenuated at large ranges. The interesting part about the two bottom paths is that their propagation loss is about equal but for different reasons. The silty clay bottom is assumed to be poorly structured so that it primarily supports P waves. This is not an unreasonable assumption; shallow water data interpretations have used this assumption with reasonable success in the past. The crystalline bottom supports both P and S waves. However, the P/S ratio of conversion is approximately 0.002 for c equal to β at 3 Hz. Therefore nearly all of the energy in the bottom is in the form of shear waves. The attenuation of shear waves is approximately 3 to 5 times that of compressional waves resulting in a decrement

21

of approximately 0.025. Thus we have the interesting situation where shear waves can provide an effective means of signal propagation. These numbers can be considered optimistic, and the controlling factor is attenuation, which increases linearly with range. Therefore, one can make the following observations:

1. Under favorable conditions the water path will yield useful signal levels at ranges of 100 km.

2. Under unfavorable water conditions the bottom path will yield a reliable range estimated to be 10 to 20 km.

2.3 Background Noise

There are few measurements of seismic background noise in shallow water. Figure 6 shows typical observed noise levels from the deep basins in the western Pacific measured by ocean bottom seismometers (OBS) (Reference 16). The particle velocity levels are in general agreement with noise measurements using hydrophones in the same general area at similar depths. Latham (Reference 17) indicates that the noise levels in shallow water are similar to those in Figure 6 except in the frequency region below 15 Hz. In shallow water the steep rise in energy begins several Hz higher in frequency than in deep water. Inferences from the small amount of data available can be misleading. However, we can conclude that the shallow water environment is no noisier than the deep sea environment except at the low frequencies. At present we do not know the directionality of

22
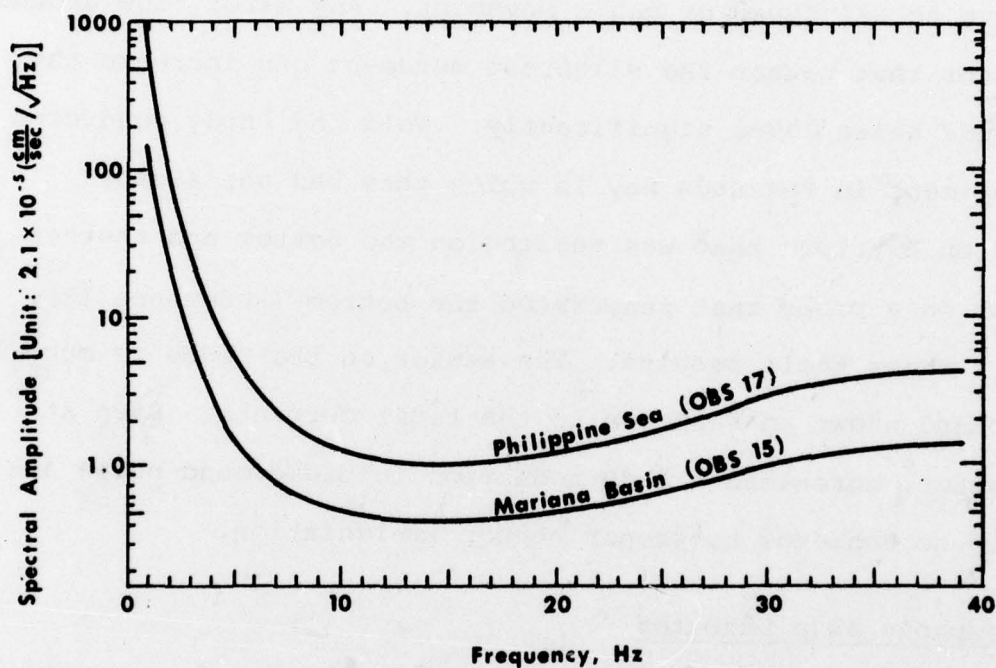
Figure 6. Typical Noise Spectra At Ocean Bottom. (After Reference 16).

Data from Site 15 (depth, 5600 m) and Site 17 (6500 m). The noise spectra and noise level seem to vary with bottom depth; however when the depth exceeds 5500 m, the noise level is comparable to the quietest places on land, for frequencies more than about 7 Hz.

the noise, whether it is omnidirectional, primarily horizontal or vertical. It is not known whether the directionality changes as a function of frequency. The answer to these questions can strongly affect the type sensor that should be used.

Since geophones are particle velocity devices, they are sensitive to all types of media movement. Any water flow around the sensor that causes the slightest movement can increase the background noise level significantly. Wold and Purdy conducted an experiment in Buzzards Bay in which they had one sensor mounted on a tripod that was resting on the bottom and another that was on a probe that penetrated the bottom (Reference 18). Figure 7 shows their results. The sensor on the probe is much quieter and shows no response to the tidal currents. Even at slack water, more than a 6 dB reduction in background noise appears to be achieved by proper sensor implantation.

2.4 Geophone as a Detector

A geophone is an electromechanical sensor based on a non-moving reference point, and a moving earth that causes a voltage to be generated. The mechanical part of the system simulates a point fixed in space by using a relatively large mass. A coil of wire is wound on the mass. Permanent magnets create a magnetic field about the coil; the magnets are attached to the earth. If the earth moves, the magnets move, the coil remains in place, and an electrical signal is generated in the coil proportional to the rate of relative motion; hence, the

24
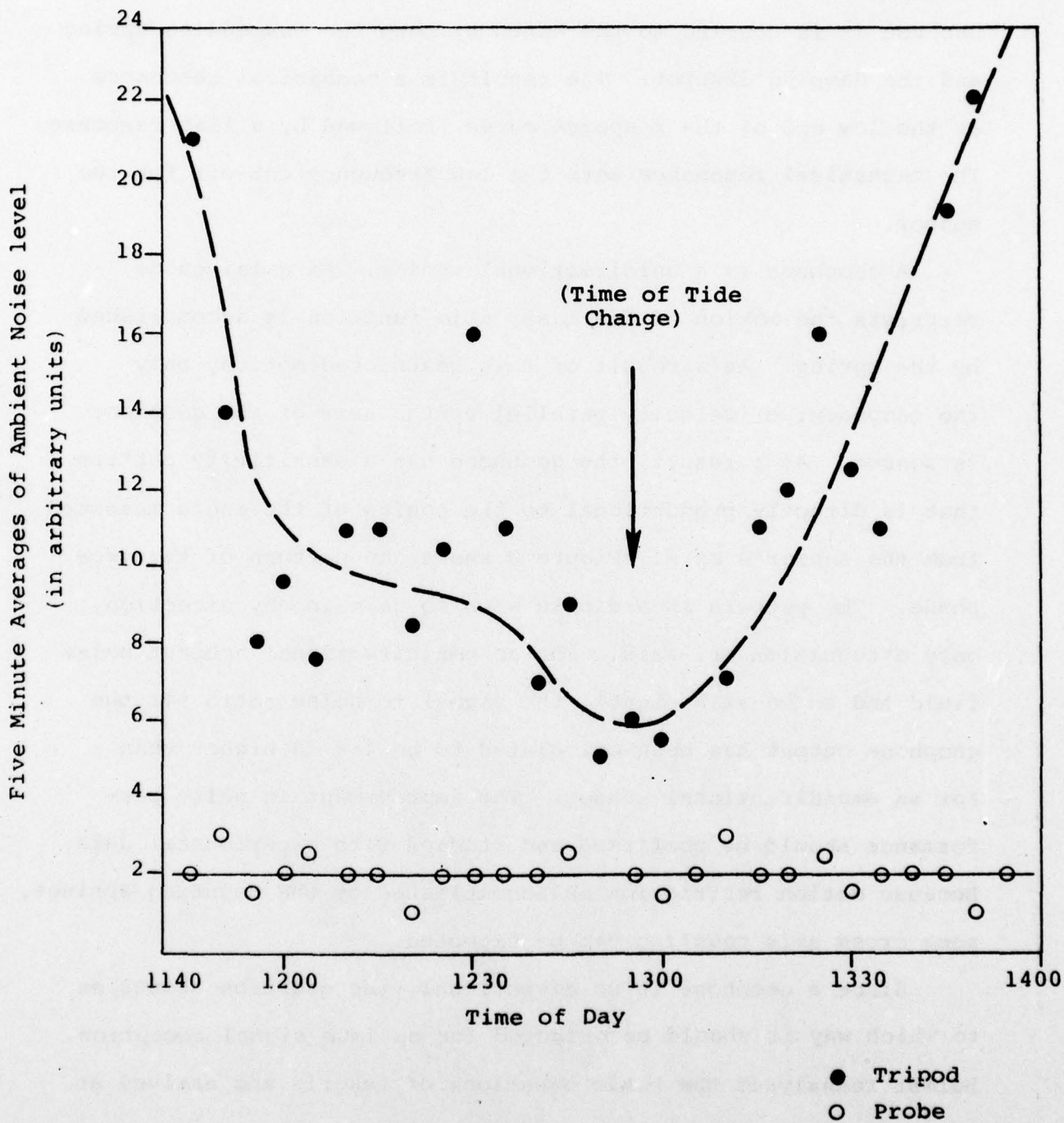
Figure 7. Background Noise Measurement Comparison between Geophones Mounted on a Tripod and on a Probe. (After Reference 18).

25

often used term velocity geophone. The above ideal system is difficult to achieve. The mass only approximates a fixed point, because it is coupled to the earth by both the suspending spring and the damping dashpot. The result is a mechanical resonance at the low end of the response curve, followed by a flat response. The mechanical resonance sets the low frequency cut-off for the sensor.

A geophone is a unidirectional sensor. An axial guide restricts the motion of the mass; this function is accomplished by the spring. As a result of this restricted motion, only the component of velocity parallel to the axis of the geophone is sensed. As a result, the geophone has a sensitivity pattern that is directly proportional to the cosine of the angle measured from the sensor's axis. Figure 8 shows the pattern of the geophone. The pattern is a dipole with no gain in any direction, only attenuation off-axis. For an omnidirectional ambient noise field and an on-axis signal, the signal to noise ratio for the geophone output has been calculated to be 4.8 dB higher than for an omnidirectional sensor. The improvement in noise performance should be confirmed and studied with experimental data. Because motion restriction is accomplished by the mounting springs, some cross axis coupling can be expected.

Since a geophone is unidirectional, the question arises as to which way it should be oriented for optimum signal reception. Holmer reanalyzed the basic equations of Pekeris and arrived at

26
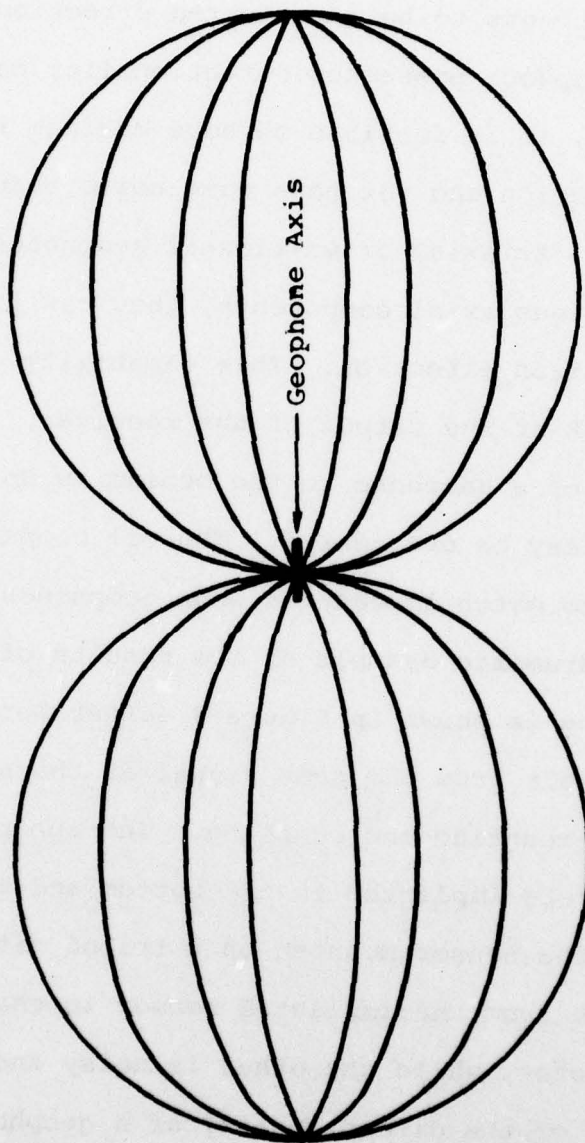
Figure 8.   Directivity Pattern of a Geophone

the conclusion that for a ratio of phase velocity to layer velocity of $\sqrt{2}$ or less the maximum particle velocity is in the horizontal direction for compressional waves (Reference Appendix B). McLeroy (Reference 12) has also demonstrated the same conclusion in one of his experiments.

Since there appears to be a preferred direction for signal arrival and the geophone possesses directionality capabilities in a small package, it is feasible to have maximum response in the signal direction and yet have some noise reduction. To accomplish this, triaxial or multiaxial geophones can be used. By phasing the various axial components, they can be electrically steered in any desired direction. This capability can be used to increase the SNR at the output of the receiver.

The coupling of a geophone to the medium is an important factor that often may be overlooked. The oil companies often take great pains to match impedances when geophones are implanted in boreholes. A dramatic example of the results of different degrees of coupling is shown in Figure 9 (after Reference 18). The two curves result from the same signal at the same range, but for different mounting and coupling. The upper curve is the result of a probe implanted in the bottom and the lower is the result of the sensor mounted on a tripod sitting on the bottom. The trace from the implanted sensor is sharp and distinct in character, while the other is noisy and indistinct.

In the light of the directionality of a geophone, let us reexamine the Fire Island data shown in Figure 3. Vertical geophones were clamped in the well at a depth of 119 meters.

Shot 21: Probe

Shot 21: Tripod

1 sec.

Figure 9. Comparative Responses of Probe- and Tripod-mounted Geophones to an Explosion (After Reference 18).

29

At a range of 2 to 20 miles one expects the signal propagation vectors to be mainly horizontal. Therefore, if horizontal geophones had been used it would be expected that the observed propagation loss would have been somewhat less, probably as much as 10 dB less.

2.5 Seismic Array Design

The potential for deriving spatial gain is dependent on the spatial and time coherence of a signal. The Large Aperture Seismic Array has demonstrated that beamforming is feasible and results in appreciable gain.

Considering the bottom as the propagation medium, we know from facies changes associated with sedimentation that the propagation medium will be spatially dependent. As a result large deviations from the plane wave assumptions will probably occur, and the wave front curvature problem will need to be effectively dealt with. In addition, the inhomogeneities near the sensors may cause serious deviation, whereas the distant ones will blend into a slowly varying simple medium. The inhomogeneity effects near the array can be calibrated in much the same manner that bottom arrays are presently calibrated.

Four potential array designs will be considered: (1) the distributed system, (2) several small aperture arrays, (3) a single large aperture array, and (4) borehole receivers. Each of these designs will be considered in turn.

The use of a distributed system is associated with areas of poor acoustic propagation. Although the propagation loss for the better propagation conditions was investigated above, there are other water and bottom conditions in which the propagation is much poorer. For these poorer conditions, the distributed system is probably the ideal system.

If the distributed system is made up of multiaxial geophones, each of these sensors can be steered and an estimated spatial gain of 3 dB may be realized. Thus each element of the distributed system is in itself a mini-array.

Previously the reliable range for propagation through the bottom was estimated at 10 to 20 km for silt clay type materials. For sand bottoms, the range will be considerably shorter. For a distributed system, a sensor separation in the range of 10 to 100 km can be anticipated depending on propagation conditions.

Small aperture arrays have several outstanding attributes for use in the shallow water environment. Small aperture is used here to limit array size to the range of 1 to 10 wavelengths.

With a small aperture the wave front distortion problem should be minimized, thus normal beamforming will yield near theoretical gain; or if special processing is required, it can be less complex than for the large aperture array.

A small aperture array has greater spatial gain per installed sensor, since the increase in array gain in dB with increasing N is proportional to $\frac{1}{N}$.

31

The use of geophones as sensors also implies special pro-
cedures for coupling each element to the bottom; therefore,
the larger part of array installation cost will be the per-
element cost. The cost per element will become a much larger
factor than with hydrophone arrays.

Another aspect is that two or more small aperture arrays
can be used for multiple array processing. The type of proc-
essing requires coherence between the arrays. The ambiguity
plane processing gives high gain for low resolution systems.
Also, the multiple array processing yields excellent localization
capability.

Even with high attenuation the use of small aperture arrays
in a multiple array processing scheme will have greater range
capability than a simple large aperture array, will concentrate
sensors in few locations as compared to a distributed system,
and will provide better localization and classification infor-
mation than the other concepts.

A large aperture array is useful for good propagation con-
ditions and for wide coherent domain media. In shallow water,
propagation loss is in the vicinity of 10 log R for optimal
environmental conditions, which are estimated to occur less
than 25% of the time and probably over less than 20% of the
eastern seaboard continental shelf. Under such conditions the
large aperture array would make only a limited contribution
to surveillance efforts. For example, a 10 Hz, 50-element
array is approximately 8 km in length for a compressional

velocity of 1600 m/s. With such a large aperture, sophisticated calibration and beamforming will be required to begin to realize the potential spatial gain. The large aperture array does not appear to be a viable concept in shallow water.

Locating geophones in boreholes is an interesting concept for two reasons: (1) the receiving location could be near the shore or on shore, and (2) the propagation loss through the bottom will be minimized. The minimization of the propagation loss is based on the higher attenuation coefficients of the unconsolidated sediments overlying the crystalline basement. The borehole concept would minimize the distance the signal traverses the sediments to the receiver, which is estimated to decrease propagation loss from several dB to as much as 10 to 15 dB. However, there are difficulties with the concept. In the Fire Island experiment, the borehole was found to resonate. and cause high level artifacts. It may be possible to use these mechanical resonant effects to advantage. Little is known about the interaction of a signal with a borehole and its possibilities in the 3-30 Hz frequency region.

Since propagation in shallow water is controlled by the size of the attenuation coefficient, a distributed system or small aperture array appears to be the most effective choice. The use of boreholes is a virgin subject and should be investigated.

2.6 Needed Measurements

Since data that demonstrates the usefulness of seismic
paths for acoustic propagation at long ranges in shallow water
is nearly nonexistent, all types of measurements are sorely
needed. However, it would appear that concentrating efforts
in the more basic areas so that a firm foundation can be estab-
lished upon which to base surveillance concepts may be a viable
basis for selecting needed measurements. Therefore, recommended
measurements should be limited to four general areas, (1) background
noise, (2) signal propagation, (3) comparative SNR, and (4)
bottom acoustic parameters.

Background noise measurements should be made at a number
of locations to quantify noise directionality and amplitude ver-
sus depth in the communication link, i.e., from the water surface
to some depth in the bottom. Comparisons of levels between
pressure and particle velocity are needed.

Numerous signal propagation measurements have been made
in shallow water, but most of these focus on the water path.
We need some measurements that quantify propagation in the sedi-
ments, to confirm both the wave theory and the attenuation
constants, many of which have been determined at relatively high
frequency.

Comparative signal to noise ratios (SNR) for hydrophones ver-
sus geophones need to be determined. At short ranges there appears
to be some benefit from using horizontal geophones. Again these

measurements need to be performed as a function of depth. One
of the purposes should be to verify the vertical velocity po-
tential predictions of normal mode theory.

The lack of bottom acoustic parameter measurements has been
recognized as the limiting factor in making propagation pre-
dictions in shallow water for a long time. The situation has
not changed. However, the issue of how to map the bottom should
be resolved before proceeding with any extensive mapping program.

3. DISCUSSION

3.1 Methodology Issues

There are many issues to be resolved before seismic prop-
agation is fully understood and its capability completely evaluated.
However there appear to be two issues that are rather basic:
(1) the acoustic description of the bottom and (2) the sensor
to medium coupling.

As previously stated the lack of applicable bottom informa-
tion makes acoustic signal predictions risky except in a quali-
tative sense. The cost of mapping the bottom is expensive.
At present, three methods of determining the parameters are being
fostered:

1. Seismic refraction measurements of layer thickness
   and velocity with density estimates.

2. The dispersion method, which determines how the bottom
   acts as a communication channel as a whole; only in-
   homogeneities that affect acoustics are determined.

3. The inference method, which involves the determination
   of the effect of the fine sedimentation structure
   on acoustics. Then the sedimentary sequences of the
   bottom are mapped in detail. From these maps the
   acoustic properties that one needs to make predictions
   are inferred.

The first thing that needs to be done is to determine which
of the above methods is the most cost-effective in conjunction
with acoustic signal prediction accuracy.

37

How to sample the communication link, i.e. the combined
water and bottom medium, is another way of stating the issue
of sensor to medium coupling. Where should the sensors be placed?
Is the velocity potential function versus depth a good indication
of vertical placement? The use of hydrophones versus geophones
as sensors is at present being investigated. Without under-
standing the effects of medium sampling, the measured results
will probably lead to contradictory conclusions. For this issue
there are more questions than answers. A geophone versus hydro-
phone receiver comparison needs to be based on physical reality
rather than on a set of measurements that can, at best, be
related statistically.

If we can gain some insight into these two issues, the under-
standing of seismic detection will take a significant step forward
and subsequent issues of importance may then be examined.

3.2 Critical Experiments

The above discussion indicates qualitatively that sound
propagation through the bottom may be of importance to the detec-
tion of ships. The analysis of the distribution of the sound
potential as a function of depth indicates that sizable amounts
of energy can be propagated in the bottom. Short range data
and theoretical analysis indicate that the horizontal geophone
may have a signal-to-noise ratio advantage over a pressure sensor
at the ranges of interest. Since there is no applicable data at

38

these ranges of interest, three experiments are proposed to determine the viability of seismic propagation in the overall ship detection scheme. The guidelines for the experiments are:

1. Both hydrophone and triaxial geophone measurements should be made for comparison.

2. Although impulsive sources may be used to define propagation loss as a function of range, the data needs to be processed so that it is applicable to CW sources such as ships.

3. Basic environmental data needs to be collected during the experiment.

4. All signal transmission paths, water and seismic, should be measured.

Experiment 1 - Signal Propagation Through A Silty Clay Bottom

Silty Clay is reported to have the lowest attenuation factor among the various sediment types. Since the eastern continental shelf is mainly composed of thick sections of sediments, this experiment will investigate a favorable acoustic environment for geophone sensors. Signal propagation runs up and down the slope as well as parallel to the slope should be made.

Experiment 2 - Signal Propagation Through A High Speed
                Crystalline Rock Bottom

The purpose of this experiment is to define propagation loss through a potentially low-loss crystalline bottom with thin sediment cover. This experiment will evaluate the use of shear

waves as an energy transmitting mechanism. In general, the higher the velocity, the lower the loss that is expected. For crystalline rock the attenuation factor per cycle is very low, approximately 0.05 dB per cycle. This experiment will investigate a potentially favorable environment for long range acoustic propagation in the bottom using geophones for sensors.

These two proposed experiments will define and quantify long range signal propagation through the bottom. Also, comparative signal to noise measurements should be made between geophones and hydrophones.

4. SUMMARY AND RECOMMENDATIONS

From the investigation it is concluded that there is
insufficient data available to determine the impact that
seismic propagation paths can have on detection capability
in shallow water. The greatest contribution that a bottom
path could make would be to furnish a reliable range of
detection that is independent of the velocity profile in the
water. Two worthwhile and critical experiments that would
better define the potential role of seismic detection are:

1. Signal propagation through a silty clay bottom
2. Signal propagation through a high speed crystalline
   rock bottom.

If these experiments indicate that seismic propagation
is a viable concept, the issues of bottom description, coupling,
and hydrophone versus geophone advantages will need to be
addressed.

REFERENCES

1. M. Ewing, J. L. Worzel, C. L. Pekeris, Propagation of Sound in the Ocean, Geological Society of America Memoir 27. October, 1948.

2. R. H. Ferris, "Comparison of Measured and Calculated Normal-Mode Amplitude Functions for Acoustic Waves in Shallow Water" JASA, Vol. 52 #3, p. 981, February, 1972.

3. A. O. Williams, Jr. "Hidden Depths: Acceptable Ignorance About Ocean Bottoms." JASA, Vol. 59 #5, p. 1175, May, 1976.

4. I. Tolstoy, "Guided Waves In a Fluid With Continously Variable Velocity Overlying an Elastic Solid: Theory and Experiment." JASA, Vol. 32 #1, p. 81, 1960.

5. E. J. Kornhauser, and W. P. Raney, "Attenuation In Shallow Water Propagation Due to an Absorbing Bottom." JASA, Vol. 27 #4, p. 689, July, 1955.

6. M. Blaik and C. S. Clay, "Detection In the Ground of Sound From a Source In Shallow Water." Hudson Laboratories Technical Report #76. 25 May, 1959.

7. I. Tolstoy, "Shallow Water Test of the Theory of Layered Wave Guides", JASA Vol. 30 #4, p. 348, April, 1958.

8. C. B. Officer, Introduction to the Theory of Sound Transmission. McGraw-Hill Book Co., 1958.

9. P. A. Barakos, "Experimental Determination of Compressional Velocity for the Bottom Layer by the Dispersive Method". JASA, Vol. 34 #12, p. 1919, December, 1962.

10. H. P. Bucker, "Normal-Mode Sound Propagation in Shallow Water" JASA, Vol. 36 #2, p. 251, February, 1964.

11. R. Houtz, J. Ewing and X. LePichon, "Velocity of Deep-Sea Sediments From Sonobuoy Data." Journal of Geophysical Research, Vol. 73 #8, p. 2615, April, 1968.

12. E. G. McLeroy and A. DeLoach, "Measurements of Sea Bottom Elastic Waves from Underwater Explosions", U.S. Navy Mine Defense Laboratory Report #U2727, April, 1966.

13. H. P. Bucker, J. A. Whitney and D. L. Keir, "Use of Stoneley Waves to Determine the Shear Velocity from Ocean Sediments." JASA Vol. 36 #8, p. 1595, August, 1964.

14. E. L. Hamilton, "Attenuation of Shear Waves in Marine Sediments", JASA, Vol. 60 #2, p. 334, May, 1976.

15. W. M. Ewing, W. S. Jardetsky, F. Press, <u>Elastic Waves in Layered Media</u>, McGraw-Hill Book Co., 1957.

16. T. Asada, and H. Shumamura, "Observation of Earthquakes and Explosions at the Bottom of the Western Pacific: Structure of Oceanic Lithosphere Revealed by Long-Shot Experiments in the Geophysics of the Pacific Ocean Basin and Its Margin" Geophysical Monograph 19, American Geophysical Union, 1976

17. G. Latham, "OBS Shallow Water Studies", Paper given at Workshop on Seismic Wave Propagation in Shallow Water, July 6 and 7, 1978.

18. R. Wold, "Private Communication".

44

APPENDIX A

DEPTH OF PENETRATION OF
ACOUSTIC ENERGY INTO THE BOTTOM

By

Louis A. Mole

The intent of this Appendix is to provide a brief intro-
ductory explanation of the theoretical treatment of the depth to
which significant amounts of energy will be present in the bottom.
The development will follow the normal mode theory approach of
Pekeris (Reference 1). The principal observed features of the
data records of sound received from an explosion in shallow
water may be explained by a model termed a two-layer half space.
In the model shown in Figure A-1, the upper layer, the water, is
a liquid with density ρ_1 and sound velocity c_1 whereas the lower
layer, the bottom, is also assumed to be a liquid of density
ρ_2 and sound velocity c_2. The problem of interest is to deter-
mine the pressure field due to an explosion in the water. For
long ranges, the disturbance can be assumed to be produced by
a point source which, in the absence of the surface and the

z = 0 _____ surface _____

d ↓

z = d   * point source

H

water ρ_1, c_1

z = H _____

bottom ρ_2, c_2
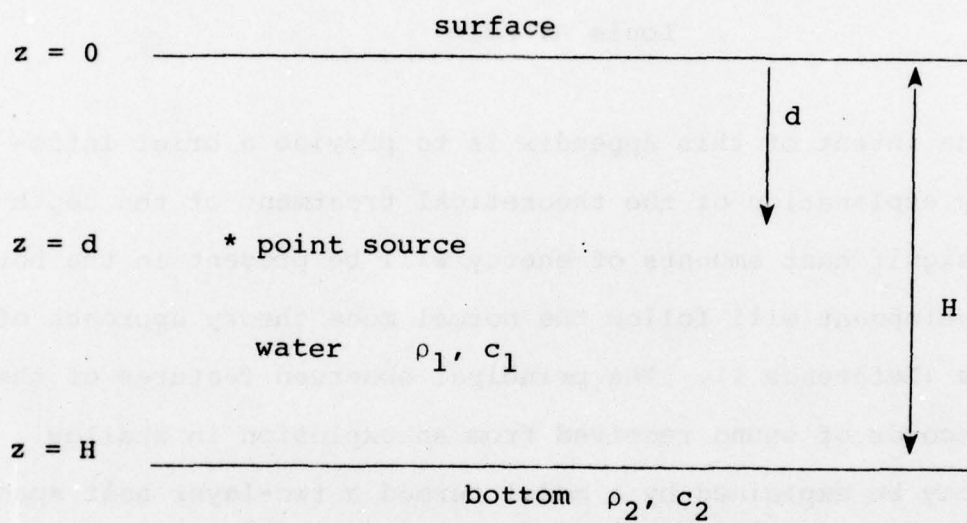
Figure A-1. Model for a Two Layered Half Space

bottom, would generate a spherically symmetrical wave whose amplitude would decrease as the inverse power of the range. However, the initially spherical wave suffers multiple reflections both at the surface and the bottom, and therefore, at long range, the number of such reflections that must be accounted for is very large. Because the requirement is to be able to compute the pressure variation at long range, for a known yield of explosive detonated at a given depth where the characteristics of the bottom are known, this necessitates that an exact solution of the wave equation be attempted.

Following Pekeris (Reference 1), the wave equation for the sound potential, ϕ, in the water and in the bottom is written as:

$$\nabla^2 \phi_1 = \frac{1}{c_1^2} \frac{\partial^2 \phi_1}{\partial t^2} \qquad 0 < z < H \text{ (water)} \qquad \text{(A-1)}$$

$$\nabla^2 \phi_2 = \frac{1}{c_2^2} \frac{\partial^2 \phi_2}{\partial t^2} \qquad z > H \text{ (bottom)} \qquad \text{(A-2)}$$

where the subscripts refer to the water and the bottom, respectively. The acoustic pressure, p, is defined as the temporal derivative of the sound potential. The horizontal and vertical components of velocity, u and w, are defined as the spatial derivative of the sound potential. These equations are expressed as:

$$p = \rho \frac{\partial \phi}{\partial t} , \quad u = - \frac{\partial \phi}{\partial r} , \quad w = - \frac{\partial \phi}{\partial z} \qquad \text{(A-3)}$$

Eqs. A-1 and A-2 must be solved subject to the following constraints: 1) the pressure should vanish at the surface, 2) at the source, the sound potential should exhibit a functional form of $f(t-r/c_1)/r$ where r is the distance from the source and $f(t)$ is the time variation of the pressure pulse, and 3) the vertical component of the velocity and pressure should be continuous across the bottom interface. Presented formally these conditions are that:

$$\phi_1 = 0 \qquad \text{at } z = 0 \qquad \qquad (A-4)$$

$$\frac{\partial \phi_1}{\partial z} = \frac{\partial \phi_2}{\partial z} \quad \text{and} \quad \rho_1 \phi_1 = \rho_2 \phi_2 \quad \text{at } z = H \qquad (A-5)$$

The solution for this problem is obtained in two steps by solving for the case when the point source is periodic of circular frequency, ω, and then generalizing the solution for an arbitrary pressure pulse $f(t)$ by a Fourier synthesis. Specifically, for an individual frequency, the sound potential is written as:

$$\phi = e^{i\omega t} \psi(r,z,\omega) \qquad \qquad (A-6)$$

and in general it is written as:

$$\phi(r,z,t) = \frac{1}{2\pi} \int_{-\infty}^{\infty} e^{i\omega t} \psi(r,z,\omega) g(\omega) \, dw \qquad (A-7)$$

where $g(\omega)$ is the spectrum of the pressure pulse, defined as:

$$g(\omega) = \int_{-\infty}^{\infty} e^{-i\omega t} f(t) \, dt \qquad \qquad (A-8)$$

A-4

The formal solution of the sound potential due to a periodic point source consists of three equations, one for each of the regions in the two-layered half space. These three equations are:

$$\psi_1 = 2 \int_0^\infty J_0(kr)\,dk \, \frac{\sin \beta_1 z}{\beta_1} \left[\frac{\beta_1 \cos \beta_1(H-d) + ib\beta_2 \sin \beta_1(H-d)}{\beta_1 \cos \beta_1 H + ib\beta_2 \sin \beta_1 H} \right] \begin{array}{l} \text{for} \\ 0 \le z \le d \end{array} \quad (A-9)$$

$$\psi_2 = 2 \int_0^\infty J_0(kr)\,k\,dk \, \frac{\sin \beta_1 d}{\beta_1} \left[\frac{\beta_1 \cos \beta_1(H-z) + ib\beta_2 \sin \beta_1(H-z)}{\beta_1 \cos \beta_1 H + ib\beta_2 \sin \beta_1 H} \right] \begin{array}{l} \text{for} \\ d \le z \le H \end{array} \quad (A-10)$$

and

$$\psi_3 = 2b \int_0^\infty J_0(kr)\,k\,dk \, \frac{\sin(\beta_1 d)\, e^{-i\beta_2(z-H)}}{(\beta_1 \cos \beta_1 H + ib\beta_2 \sin \beta_1 H)} \quad \text{for } z \ge H \quad (A-11)$$

At each of the boundaries, $Z=d$ and $z=H$, the equations are continuous. In addition, the following terms are also defined:

$$b = \rho_1/\rho_2 \quad (A-12)$$

$$\beta_n = \sqrt{\omega^2/c_n^2 - k^2} \qquad k < (\omega/c_n) \quad (A-13)$$

$$= -i\sqrt{k^2 - (\omega^2/c_n^2)} \qquad k > (\omega/c_n) \quad (A-14)$$

Formal evaluation of these terms can only be profitably made by transforming the path of integration into the complex k plane. At long range, the only terms remaining from the integration are the residues from the integrands, which are usually termed the normal modes. Therefore, for long range, the asymptotic form of the solution may be written as:

$$\phi' = \left(\frac{2\pi}{H}\right) b_0 \sqrt{\frac{2}{\pi r}} \sum_{n=1}^{\infty} \frac{1}{\sqrt{k_n}} \; e^{i[\omega t - k_n r - (\pi/4)]} \; F(x_n) \; \phi_n(d) \; \phi_n(z) \quad \text{(A-15)}$$

where

$$\phi_n(d) = \sin (x_n d/H) \quad\quad\quad\quad\quad\quad\quad\quad \text{(A-16)}$$

and

$$F(x_n) = \frac{x_n}{(x_n - \sin x_n \cos x_n - b^2 \sin^2 x_n \tan x_n)} \quad \text{(A-17)}$$

Eq. A-15 has two forms depending on the depth factor z. This depends on the two terms:

$$b_0 = 1 \quad\quad\quad\quad 0 < z < H \quad\quad\quad\quad\quad\quad \text{(A-18)}$$

$$= b \quad\quad\quad\quad z > H \quad\quad\quad\quad\quad\quad\quad \text{(A-19)}$$

and

$$\phi_n(z) = \sin (x_n z/H) \quad\quad 0 < z < H \quad\quad\quad\quad \text{(A-20)}$$

$$= \sin (x_n) \; e^{\sqrt{k_n^2 - \omega^2/c_2^2}(z-H)} \quad\quad z > H \quad \text{(A-21)}$$

The x_n are roots of the equations:

$$x_n = H \sqrt{\frac{\omega^2}{c_1^2} - k_n^2} \quad\quad\quad\quad\quad\quad\quad\quad \text{(A-22)}$$

or:

$$\frac{\tan x_n}{x_n} = \frac{-1}{bH\sqrt{k_n^2 - \frac{\omega^2}{c_2^2}}} \quad\quad\quad\quad\quad\quad \text{(A-23)}$$

A-6

The factor $e^{i(\omega t - k_n r)}$ in Eq. A-15 gives a very obvious inter-
pretation of k_n namely that $k_n = \omega/c_n$, where c_n denotes the
phase velocity of the nth normal mode. The meaning of phase
velocity is that, in case of an arbitrary disturbance, the
amplitude of the Fourier spectrum of the disturbance at ω is
propagated with the speed of the phase velocity. The phase
velocity of the normal modes starts at the cutoff frequency
with the value of the speed of sound in the bottom and decreases
continuously with increasing frequency toward the value of sound
velocity in the water. For an arbitrary disturbance, the low
frequency components in the spectrum of a pressure pulse would
get ahead of the high frequency components, so that at long
range, the received pulse would appear in the form of a train
of nearly sinusoidal waves in which the period decreases with
time. The factor,

$$e^{i[\omega t - k_n r - (\pi/4)]} \sin(x_n z/H) \tag{A-24}$$

in Eq. A-15 indicates that the normal modes can be decomposed into
two plane waves, one traveling obliquely upward and the other
downward.

The factor $\phi_n(z)$ in Eq. A-15 represents the amplitude of
the nth normal mode. When $c_2 > c_1$ the roots of Eqs. A-22 and A-23
are real, whereas when $c_2 < c_1$ the roots are complex and imaginary.
In the latter case, the factor $e^{-ik_n r}$ implies horizontal attenu-
ation, whereas in the case of a fast bottom, there exist solutions
which suffer no horizontal damping. For angles of incidence
greater than the critical angle, no power is transmitted into

A-7

the bottom. For the first mode, the amplitude decreases expo-
nentially with depth below the bottom and as the frequencies
become higher, on the order of 1 kHz, very little of the
energy in the first mode is left in the bottom. One consequence
of this weakening of penetration of the energy of the first
mode into the bottom, with increasing frequency, is that ob-
servations (or dispersion) of high frequencies can yield
little information on the nature of the bottom.

As a measure of the depth of penetration of the first
mode into the bottom, a layer at the top of the bottom is
defined, which contains 99% of the total energy in the bottom.
The significance of the depth of pentration is that no infor-
mation on the structure of the bottom at greater depths can
be obtained from dispersion data. The equation for the pene-
tration depth may be derived from Eq. A-21 in the following
manner.

An expression will now be developed to calculate pene-
tration depth explicitly. The depth at which 99% of the energy
in the bottom is above that particular depth is equivalent to
determining the depth at which the pressure amplitude is 0.1
of the value at the bottom (z=H). If the exponential portion of
Eq. A-21 is equated to 0.1, then the logarithm of the result is:

$$-i\beta_2 (z-H) = -2.3026 \qquad (A-25)$$

Using Eq. A-14, the result becomes:

$$(z-H) \sqrt{k_n^2 - \frac{\omega^2}{c_2^2}} = -2.3026 \qquad (A-26)$$

A-8

If a dimensionless quantity, γ, relating frequency, depth and velocity, is defined as follows:

$$\gamma = \frac{\omega H}{2\pi c_1} \tag{A-27}$$

then Eq. A-26 can be rewritten as:

$$\gamma \left(\frac{z}{H} - 1\right) = \frac{(.36647)}{\sqrt{\dfrac{c_1^2}{c_n^2} - \dfrac{c_1^2}{c_2^2}}} \tag{A-28}$$

Eq. A-28 can be used to calculate the penetration depth for specific discrete values of c_n where the constraint on c_n is that $c_1 < c_n < c_2$. In order to determine the appropriate value of c_n, the equation for x_n must be solved, i.e. either Eq. A-22 or A-23.

If a large depth of penetration is defined as a depth greater than the water depth, then for most velocity ratios, $\frac{c_1}{c_2} < 0.95$, large depths of penetration will be confined to areas with water depths of less than 2λ. Hence, the lower frequency energy will couple deeper into the bottom.

APPENDIX B

RELATION OF PARTICLE VELOCITY AND PRESSURE
IN A TWO-LAYER SHALLOW WATER AREA

By

Curtis I. Holmer

Geophones are inherently directional devices which respond to the magnitude of vector particle velocity along the geophone axis associated with acoustic propagation in a medium. As a result of this directional response, a significant question with regard to system performance analysis is that of determining an appropriate placement of the axis of maximum sensitivity for signal detection. The fact that no universal answer to this question has appeared in the literature points to the complexity of the problem. In this appendix, we will derive some general answers to this question for the particular case of low-frequency, shallow-water propagation in a two-layer half-space, through systematic analysis of an analytic model. While the velocity is sensitive to the frequency range of interest, water depth, bottom properties and source range, it will be shown that the relationship of velocity to pressure, as well as the relationship between velocity components is easily statable. The discussions to follow are based on the analytic model of a two-layer half-space developed by Pekeris (Reference 1).

Liquid Bottom

Figure B-1 shows the geometry of the problem of interest. The model assumes a liquid (layer 1) of depth H, density ρ_1.
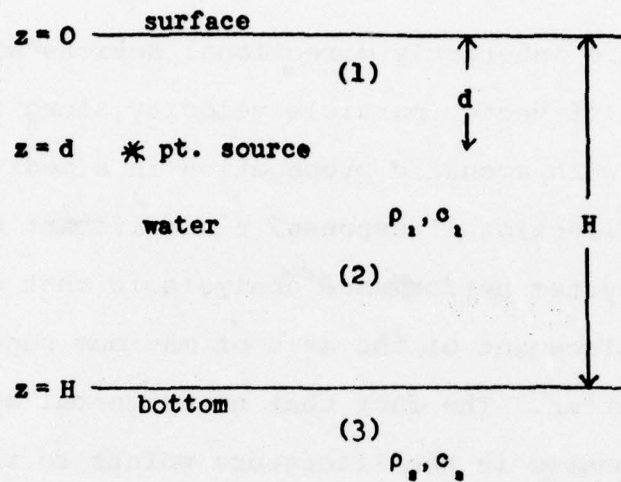
Figure B-1. Assumed Model for a Two-Layered Liquid
Half-Space

constant sound speed c_1 overlying a second liquid (layer 2)
of density $\rho_2 > \rho_1$, constant sound $c_2 > c_1$. The acoustic
source is assumed to be in the upper liquid, and our interest
is in the sound field which occurs in either layer. This
model is so highly idealized that dependence on it for highly
quantitative information is inappropriate, but we believe
that it is useful for answering qualitative questions of
the type of interest here.

The second (infinite depth) liquid layer is widely used
to represent the properties of unconsolidated sediments and
is adequate for the purposes of this discussion.

Numerous authors have solved this particular problem in detail
so we quote the appropriate expressions from Pekeris (Reference 1),
which is widely available, rather than duplicate that analysis. The
acoustic field may be described by a velocity potential which
may be written as the product of the three functions as:

$$\phi(r,z,t) = \Phi(r)W(z)X(\omega t) \tag{B-1}$$

from which we can derive both pressure and velocity expressions
according to:

$$p = \rho \frac{\partial \phi}{\partial t}, \quad u = \frac{-\partial \phi}{\partial r}, \quad w = \frac{-\partial \phi}{\partial z} \tag{B-2}$$

where p is the acoustic pressure, u and w are the horizontal
and vertical components of particle velocity respectively. The
potential ϕ for this problem has the solution:

$$\phi = \begin{array}{l} \phi'_1 + \phi''_1 \text{ for } z < H, \ (c_1 < c_2) \\ \phi'_2 + \phi''_2 \text{ for } z > H, \ (c_1 < c_2) \end{array} \tag{B-3}$$

where ϕ'_1 and ϕ'_2 may be interpreted as a sum of cylindrically spreading modes which represent the energy which is "guided" in the first layer, and have an exponentially decreasing "penetration" into the second layer. The terms ϕ''_1 and ϕ''_2 may be interpreted as arriving from a spherically spreading dipole near-field. Since we will be interested primarily in longer range propagation, we show here only those long range asymptotic forms (valid for $r > H$, where the arrow $\rightarrow$ indicates asymptotic to for large $k_n r$), i.e.:

$$\phi'_1 \rightarrow \frac{2\pi}{H} \sum_{n=1}^{\infty} \Phi_1(r,n) \, W_1(z,n) \, X_1(\omega),$$

$$\phi'_2 \rightarrow \frac{2\pi b}{H} \sum_{n=1}^{\infty} \Phi_2(r,n) \, W_2(z,n) X_2(\omega t)$$

(B-4)

where $\Phi_1(r,n) = \Phi_2(r,n) = \sqrt{\dfrac{2}{\pi k_n r}} \; e^{-i\left(k_n r - \frac{\pi}{4}\right)}$

$$X_1(\omega t) = X_2(\omega t) = e^{i\omega t} \, F(x_n) \, \sin\!\left(\frac{x_n d}{H}\right)$$

$$W_1(z,n) = \sin\!\left(\frac{x_n z}{H}\right) \qquad , \quad z < H$$

$$W_2(z,n) = \sin\!\left(x_n\right) e^{-\beta_2(n)(z-H)} \qquad , \quad z > H$$

$$F(x_n) = x_n / (x_n - \sin x_n \cos x_n - b^2 \sin^2 x_n \tan x_n)$$

$$x_n \equiv \beta_1(n) H = H\sqrt{\frac{\omega^2}{c_1^2} - k_n^2}$$

$$\beta_2(n) = \sqrt{\frac{\omega^2}{c_2^2} - k_n^2} = -i\sqrt{k_n^2 - \frac{\omega^2}{c_2^2}}$$

$$b = \rho_1/\rho_2 < 1$$

x_n are roots of the equations:

$$\frac{\tan x_n}{x_n} = \frac{i}{bH\beta_2(n)} = \frac{-1}{bH\sqrt{k_n^2 - \frac{\omega^2}{c_2^2}}}, = \frac{-1}{bH\sqrt{\frac{\omega^2}{c_1^2} - \frac{\omega^2}{c_2^2} - \frac{x_n^2}{H^2}}}$$

k_n is the horizontal component of mode wave number

$k_n = \omega/c_n$, c_n is the phase velocity of the nth mode.

$$c_n = c_1\sqrt{1 + x_n^2/k_n^2 H^2}$$

Also,

$$\phi''_1 \rightarrow \frac{2ibk_2}{(k_1r)^2} \frac{\sin(k_1d\mu)\sin(k_1z\mu)e^{-ik_2r + i\omega t}}{\mu^2\cos^2(k_1H\mu)}$$

$$\phi''_2 \rightarrow \frac{2ibk_2}{(k_1r)^2}e^{i\omega t} \frac{\sin(k_1d\mu)[k_1(z-H)\mu\cos(k_1H\mu)+b\sin(k_1H\mu)]}{\mu^2\cos^2(k_1H\mu)} \qquad (B-5)$$

$$K_1 = \omega/\bar{c}_1, \quad \bar{K}_2 = \omega/c_2, \quad \mu = \sqrt{1 - c_1^2/c_2^2}$$

K_1, K_2 are wave numbers in the infinite fluids 1 and 2, not mode wave numbers.

The above expressions, while completely describing the phenomena associated with propagation in the two layer liquid model, are too complex for our purposes. We seek to identify situations where trends may be perceived more easily. First, we observe that for some large value of k_1r, that:

$$\phi'_1 >> \phi''_1$$

$$\phi'_2 >> \phi''_2$$

B-5

and further that the ratios $\dfrac{u}{p}$ and $\dfrac{w}{p}$ may be more easily studied than u and w alone. Thus from B-2:

$$\frac{u}{p}\bigg|_{z=z_r} \simeq -\frac{\partial \phi_i'}{\partial r}\bigg/ \rho_i \frac{\partial \phi_i'}{\partial t}\bigg|_{z=z_r} \qquad i = \begin{cases} 1 & z_r < H \\ 2 & z_r > H \end{cases}$$

$$\frac{w}{p}\bigg|_{z=z_r} \simeq -\frac{\partial \phi_i'}{\partial z}\bigg/ \rho_i \frac{\partial \phi_i'}{\partial t}\bigg|_{z=z_r} \qquad\qquad\qquad \text{(B-6)}$$

Performing the indicated operations for an individual mode using Eq. B-4 and simplifying yields

$$\frac{u_n}{p_n}\bigg|_{z<H} = \frac{-\left(-\dfrac{1}{2r} - ik_n\right)\phi_1'}{\rho_1\, i\omega\phi_1'} \; ; \qquad z_r < H \qquad \text{(B-7a)}$$

$$= \frac{k_n}{\rho_1\omega}\left(1 + \frac{1}{2ik_nr}\right) \to \frac{k_n}{\rho_1\omega}$$

$$= \frac{1}{\rho_1 c_1}\left(\frac{k_n}{k_1}\right)\left(1 + \frac{1}{2ik_nr}\right) \to \frac{1}{\rho_1 c_1}\left(\frac{k_n}{K_1}\right)$$

$$\frac{u_n}{p_n}\bigg|_{z>H} = \frac{-\left(-\dfrac{1}{2r} - ik_n\right)\phi_2'}{\rho_2\, i\omega\, \rho_2'} \; ; \qquad z_r > H \qquad \text{(B-7b)}$$

$$= \frac{1}{\rho_2 c_2}\left(\frac{k_n}{K_2}\right)\left(1 + \frac{1}{2ik_nr}\right) \to \frac{1}{\rho_2 c_2}\left(\frac{k_n}{K_2}\right)$$

$$= \frac{b}{\rho_1 c_1}\left(\frac{k_n}{K_1}\right)\left(1 + \frac{1}{2ik_nr}\right) \to \frac{b}{\rho_1 c_1}\left(\frac{k_n}{K_1}\right)$$

$$= b\, \frac{u_n}{p_n}\bigg|_{z_2 H}$$

B-6

$$\frac{w_n}{p_n}\Bigg|_{z<H} = - \frac{\dfrac{x_n}{H}\dfrac{\cos(x_n z/H)}{\sin(x_n z/H)}\ \phi'_1}{\rho_1 i\omega\ \phi'_1} \tag{B-8a}$$

$$= \frac{1}{i\rho_1\omega}\ \frac{x_n/H}{\tan(x_n z/H)}$$

$$= \frac{-1}{\rho_1\omega}\ \frac{\beta_1(n)}{\tan(x_n z/H)}$$

$$= \frac{-i}{\rho_1 c_1}\ \frac{1 - k_n^2/K_1^2}{\tan(x_n z/H)}$$

$$\frac{w_n}{p_n}\Bigg|_{z>H} = - \frac{\left(-\beta_2(n)\ \phi'_2\right)}{\rho_2\ i\omega\ \phi'_2} \tag{B-8b}$$

$$= \frac{-i}{\rho_2\omega}\ \beta_2(n) = \frac{-i}{\rho_2 c_2}\ \frac{\beta_2(n)}{K_2}$$

$$= \frac{-i}{\rho_2 c_2}\ 1 - \frac{k_n^2}{K_2^2}$$

Interpretation

To improve the visibility of the parametric dependencies described by Eqs. B-7 and B-8, we note that the mode wave number k_n can be viewed as a vector component of the fluid wave number K_1. Replacing the ratio k_n/K_1 by $\sin\theta_1$ where $\theta_1 = \sin^{-1}k_n/K_1 =$

$\sin^{-1}(c_1/c_n)$. (The angle θ_1 will be interpreted physically in a following paragraph.) We observe then that the expression:

$$\sqrt{1 - \frac{k_n^2}{K_1^2}}$$

can be replaced by $\cos \theta_1$. Eqs. B-7 and B-8 are then rewritten as:

$$\frac{u_n}{p_n}\bigg|_{z<H} = \frac{1}{\rho_1 c_1}\ \sin \theta_1 \tag{B-9a}$$

$$\frac{u_n}{p_n}\bigg|_{z>H} = \frac{1}{\rho_2 c_2}\ \sin \theta_2 = \frac{b}{\rho_1 c_1}\ \sin \theta_1 \tag{B-9b}$$

$$\frac{w_a}{p_n}\bigg|_{z<H} = \frac{-i}{\rho_1 c_1}\ \frac{\cos \theta_1}{\tan(x_n z/H)} \tag{B-10a}$$

$$\frac{w_n}{p_n}\bigg|_{z>H} = \frac{-i \cos \theta_2}{\rho_2 c_2} = \frac{-ib}{\rho_1 c_1}\ \cos \theta_1 \tag{B-10b}$$

Manipulation of the terms in Eq. B-10a using the definitions following Eq. B-4 will show that this expression reduces to Eq. B-10b at $z = H$, indicating that the boundary conditions of continuity of vertical velocity at the boundary are preserved. The tangent term in the denominator of Eq. B-10a serves to relate the mode shapes of pressure and vertical velocity, i.e. that minima in sound pressure produce maxima in velocity, etc.

The expressions in Eqs. B-9 and B-10 suggest a coherent interpretation of the velocity field in the fluid as being composed of that from traveling waves, with ray paths traveling

at the angles $\pm\ \theta$ from the vertical. Thus θ represents the
mode angle. θ equals the critical angle for the bottom at the
frequency of mode cutoff, and increases smoothly with increasing
frequency to 90° from the vertical at very high frequency.
In the water column, the component of velocity in the hori-
zontal direction is simply the vector component in that direc-
tion modulated by its proportionality to the pressure. The
vertical component is a similarly modulated vector component
(but "out-of-phase", both instantaneously as indicated by the i
in the ratio and in the sense of having a maximum at pressure
minima and vice versa). Turning to the lower fluid, we note
a similar vector component type interpretation of Eqs. B-9b
and B-10b. The magnitude of the horizontal component of
velocity is merely the magnitude in the upper fluid at the
interface scaled by the density ratio $b = (\rho_1/\rho_2)$.

From the above interpretation, we can see that for mode
angles in the upper fluid which are greater than 45°, that the
velocity component in the horizontal direction in both fluids
will be greater than those in the vertical. If the critical
angle for the bottom is greater than 45° (i.e., $\frac{c_2}{c_1} < 1.41$) then
the horizontal component is greater than the vertical for all fre-
quencies, while for large velocity contrasts, we have for low
frequencies in a given mode (i.e., such that: $1.41 < \frac{c_n}{c_1} \leq \frac{c_2}{c_1}$)
that the vertical component is larger, but a transition (at
the frequency where $c_n = 1.41\ c_1$) to larger components in the

horizontal direction. In any case the magnitude of both components is modulated by the magnitude of the pressure in the mode at the depth of interest. As a fraction of the maximum pressure in the mode, the magnitude of the pressure at a constant depth in the second fluid decreases with increasing frequency (above mode cutoff). Fig. B-2 presents mode pressure distributions for the first mode at several frequencies, from which the decrease in pressure for a constant position in the second fluid with increasing frequency is apparent.

From the above analysis we conclude the following:

- The components of velocity in an underlying fluid in shallow water have magnitudes which are simply related to the pressure in the mode and the mode angle.

- For small velocity contrasts ($\frac{c_2}{c_1} < 1.41$), or for mode angles greater than 45° from vertical with any velocity contrast, the magnitude of horizontal component of velocity is always greater than the vertical component at the same depth in the underlying fluid.

The significance of this analysis for system analysis is that a horizontal geophone may be used as a selective means for viewing the acoustic energy in a mode. This may provide operational advantages in terms of signal to noise ratio since the environment may operate selectively to reduce the magnitude of noises from other sources relative to the preferred signal.
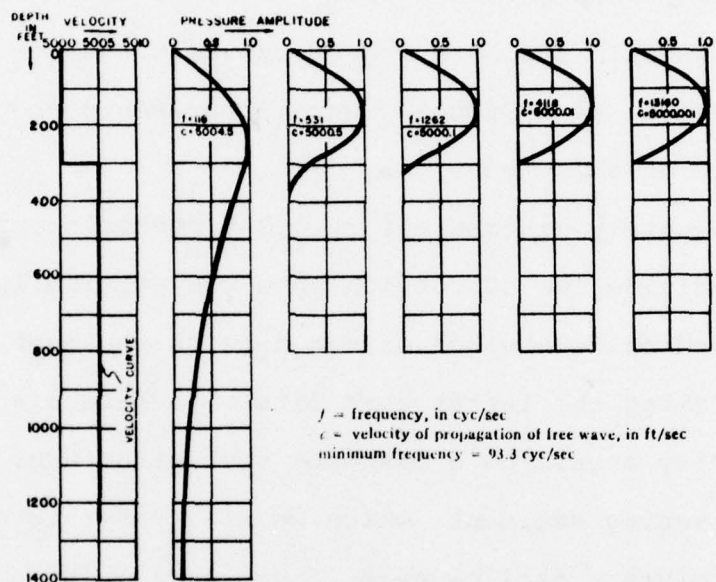
Figure B-2. Vertical Distribution of Pressure Amplitude in
the Fundamental Mode of the Free Wave.

f = frequency, in Hz
c = velocity of propagation of free
wave in ft/sec
minimum frequency = 93.3 Hz
(After Pekeris, Reference 1.)

(The example plotted here is for $\rho_1 = \rho_2$ but similarly shaped
distributions may be expected for unequal densities.)

Solid Bottom

The influence of an elastic bottom on the propagation of sound in a shallow water area is significant when compared to a liquid model bottom because of the introduction of a new mode of energy propagation, the $m = 0$ mode, which reduces to a Rayleigh wave in the zero frequency limit. A new interface wave referred to as a Stoneley wave, represents the high frequency limit of this mode.

To adequately discuss all relevant phenomena, it is desirable to subdivide the discussion into two physically different cases, depending on whether or not a thick sediment layer is present. Taking the latter case first, we have a shallow water layer directly overlying a basement rock structure, with little or no intervening sediment, which we will refer to as Case I. Case II involves a shallow water layer, overlying a shallow to deep sediment layer which further overlies a basement rock structure.

In Case I, due to the lack of a significant pressure variation component in the sound speed profile in shallow water, the sound speed variations through the column are sufficiently small so that the layer can be treated as homogeneous (as in the liquid) bottom case. The following discussion is based on the development of this model by Ewing, Jardetsky and Press (Reference 15).

The presence of the solid bottom introduces, through coupling via Poisson's ratio contraction, two different wave types in the solid. These wave types are described as volume changing (i.e. dilatational, longitudinal or P waves) and volume preserving (shear or S waves). The P waves are characterized by alternating strains along the direction of wave propagation with a characteristic speed of propagation c_ℓ in the solid. The analysis for the liquid bottom above is entirely applicable to this P wave type for modes above the first (m=0), since the longitudinal wave is the same wave form in a liquid or a solid. In addition to the previous analysis, the new m=0 mode type should be added. This mode is characterized by no low frequency cutoff, but a definite high frequency cutoff and transition to the Stoneley wave type at a frequency where the water column is on the order of 2-5 wavelengths deep. Above this frequency the mode propagates in the interface between the water and solid at a speed slightly less than the speed of sound in the water. It is characterized by exponentially-attenuating amplitude away from the interface in both media, and implies a mode angle of 90° (from the vertical). Beyond this mode, the correspondence to the liquid bottom case is complete.

The S wave on the other hand exhibits material strains (and hence response velocities) that are perpendicular to the direction of wave motion and travel at a speed c_s, which is significantly slower than c_ℓ for the same material. For the S wave type the inverse of the analysis for the liquid bottom applies (i.e. interchange $\cos \theta_1$ and $\sin \theta_1$ in the expressions for u and w).

The determination of relative magnitude of vertical and horizontal motion is more complex because of the need to consider the relative strengths of P and S wave excitation into the solid medium, which depends on the relative velocities of the two wave types in comparison with the phase speed of a mode in the water layer (i.e. c_n/c_ℓ and c_n/c_s). For Case I (i.e. homogeneous basement formation under a homogeneous liquid), and typical basement properties, the speed of both wave types is much higher than c_n so that the above ratios are small in comparison with unity. In this extreme both wave types are excited approximated equally, with the result that vertical and horizontal motions are approximately equal. The magnitudes in each of the two directions are equal with a 90° phase difference, when the deformation is induced by the guided pressure wave in the overlying fluid. Both deformations in the solid decay with an exponentially-decreasing amplitude away from the fluid-solid interface as in the liquid bottom case.

The above simple picture does not hold for solid-fluid systems where the fluid sound speed is comparable in magnitude with the shear wave speed in the solid. The Case II introduced earlier meets this latter situation, since the water and sediment layers can be modeled as an inhomogeneous liquid (i.e. with density and sound speed varying through the fluid). The case is of considerable academic interest and was studied in detail by Tolstoy, (Reference 4) but we strongly suspect that it is of little practical interest for long range detection. This assertion is

justified by the considersation that close matching of the wave
speed in the fluid with that in the underlying medium, which is
necessary for good coupling, implies significant energy loss
into this medium, resulting in rapid attenuation with range,
so that long range detection will be prohibited by signal-to-
noise ratio considerations.

To summarize the qualitative results of this section, when
a fluid overlies a homogeneous elastic half space, and sound
speeds in the solid are high with respect to the fluid, particle
velocities in the solid resulting from a signal propagation in
the fluid are equal in magnitude in both vertical and horizontal
directions.

The above conclusion might then suggest that the geophone
orientation does not matter, but it is clear that the response
of a geophone to noise sources in a direction away from the source
is not the same for horizintal vs vertical orientation. In
particular, noise sources perpendicular to the geophone axis in
the horizontal configuration would be discriminated against for
P wave direction, while this would not be the case for the ver-
tical geophone. Thus signal and noise considerations together
imply that the horizontal geophone is more appropriate for long
range detection, as in the case of the fluid bottom.

APPENDIX C

AN ANALYSIS OF SOUND PROPAGATION
IN A THREE-LAYERED LIQUID HALF SPACE

By

Louis A. Mole

Although a large number of authors treat the mathematics of the three layered liquid half space, few provide a detailed and explicit analysis of all aspects of theory of the normal mode solution in three layers. The intent of this appendix is to develop explicitly the functional form of the sound velocity potential equations for each of the three layers. The analysis for the three layered liquid is analogous to that of the two layer case as will become apparent in the ensuring paragraphs. The starting point for the mathematical analysis will be the definition of the problem in the terms with which it was formulated by Pekeris (Ref. 1).

The model, shown in Fig. C-1, consists of three liquids which are characterized by 1) densities of ρ_1, ρ_2 and ρ_3, and 2) sound velocities of c_1, c_2 and c_3, respectively. The thickness of the first layer, near the surface, is H and that of the second layer is h. A point source of singular frequency, ω, is located in the first layer at a depth d below the surface. The problem to be analyzed in this appendix is the determination of the sound velocity potential at any point in the half-space. The sound velocity potential, ϕ, from which the acoustic pressure

z = 0 ——————— surface

z = d · point source

ρ_1, c_1

H

water

z = H ———————

ρ_2, c_2

h

z = H+h ——————— bottom ρ_3, c_3
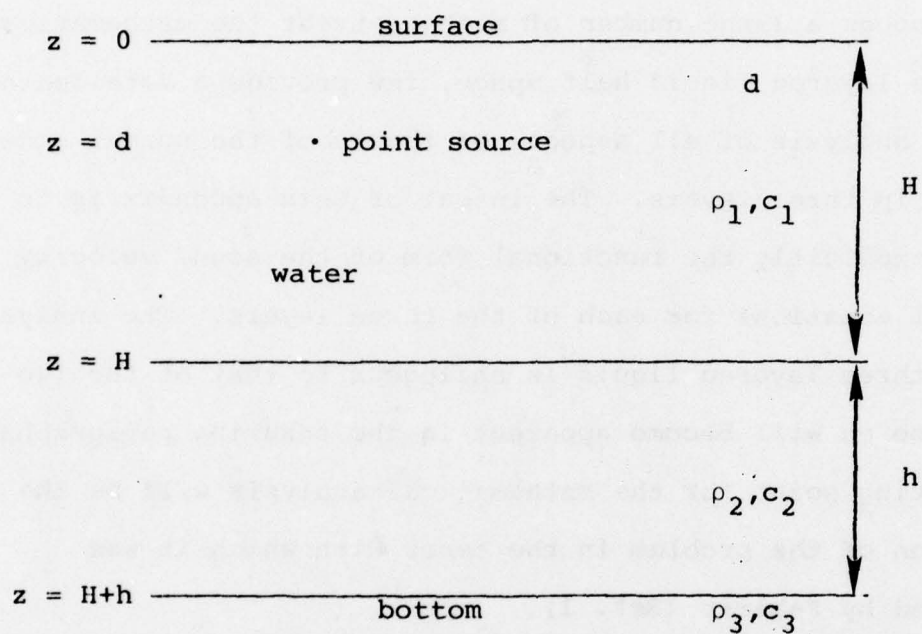
Figure C-1. Model for a Three-Layered Half Space.

and the horizontal and vertical components of the velocity may be determined, satisfies the wave equation:

$$\nabla^2 \phi = \frac{1}{c^2} \frac{\partial^2 \phi}{\partial t^2} \qquad\qquad (C-1)$$

where c is the sound velocity in one of the three layers. In order that the solution be valid everywhere in the half space, the sound velocity potential must be zero at the surface ($z = 0$) and asymtotically approach zero at infinity ($z \to \infty$). In addition, at the boundaries, $z=H$ and $z=H+h$, the vertical component of the velocity and the pressure must be continuous. To satisfy these conditions, the solution must be of the form:

$$\phi = e^{i\omega t} J_0(kr) \; F(z) \; G(k) \qquad\qquad (C-2)$$

where k is an arbitrary parameter introduced for convenience for the contour integration in the complex k plane.

If Eq. C-2 is substituted into Eq. C-1 the solution is just:

$$\frac{d^2 F_n}{dz^2} + \beta_n^2 \, F_n(z) = 0 \qquad n = 1,2,3 \qquad (C-3)$$

where

$$\beta_n = \sqrt{\frac{\omega^2}{c_n^2} - k^2} \qquad k < \frac{\omega}{c_n} \qquad\qquad (C-4)$$

and

$$\beta_n = -i\sqrt{k^2 - \frac{\omega^2}{c_n^2}} \qquad k > \frac{\omega}{c_n} \qquad\qquad (C-5)$$

C-3

The subscript n refers to the upper, middle or lower layers, i.e., n = 1,2 or 3. The subscript 1 represents the section of the upper layer below the source and 1' represents the section of the upper layer above the source. The boundary conditions for the model require that:

$$\frac{dF_1'}{dz} - \frac{dF_1}{dz} = 2k, \qquad F_1' = F_1 \text{ at } z = d \qquad \text{(C-6)}$$

$$\dot{F}_2 = \dot{F}_1, \quad \rho_2 F_2 = \rho_1 F_1 \qquad\qquad \text{at } z = H \qquad \text{(C-7)}$$

and

$$\dot{F}_3 = \dot{F}_2, \quad \rho_3 F_3 = \rho_2 F_2 \qquad\qquad \text{at } z = H + h \qquad \text{(C-8)}$$

with the understanding that the solution, Eq. C-2, must be integrated with respect to k from 0 to ∞.

For each of the layers, the solution of Eq. C-3 requires that:

$$F_1' = A \sin \beta_1 z \qquad\qquad\qquad\qquad\qquad \text{(C-9)}$$

$$F_1 = B \sin \beta_1 z + C \cos \beta_1 z \qquad\qquad\qquad \text{(C-10)}$$

$$F_2 = D \sin \beta_2 z + E \cos \beta_2 z \qquad\qquad\qquad \text{(C-11)}$$

$$F_3 = E \sin e^{-i\beta_3 z} \qquad\qquad\qquad\qquad \text{(C-12)}$$

where A, B, C, D and E are arbitrary constants which depend on the boundary conditions and strength of the source. If Eqs. C-6 thru C-8 are used with Eqs. C-9 thru C-12 to eliminate these constants, the appropriate integral equations for ϕ_1', ϕ_1, ϕ_2 and ϕ_3 can be obtained. However, for convenience, the following definitions must be made:

C-4

$$x = \beta_1 H \tag{C-13}$$

$$b = \rho_1/\rho_2 \tag{C-14}$$

$$g = \rho_2/\rho_3 \tag{C-15}$$

$$S = \frac{g\beta_3 \tan(\beta_2 h) - i\beta_2}{g\beta_3 + i\beta_2 \tan(\beta_2 h)} \tag{C-16}$$

and

$$V = \beta_1 S \cos x + b\beta_2 \sin x \tag{C-17}$$

Then the formal solutions for the sound velocity potential in the various layers are:

$$\phi_1' = 2e^{i\omega t} \int_0^\infty J_0(kr)\, kdk\, \frac{\sin \beta_1 z}{\beta_1 V} \cdot$$
$$[S\beta_1 \cos \beta_1 (H-d) + b\beta_2 \sin \beta_1 (H-d)], \quad 0<z<d \tag{C-18}$$

$$\phi_1 = 2\, e^{i\omega t} \int_0^\infty J_0(kr)\, kdk\, \frac{\sin \beta_1 d}{\beta_1 V} \cdot$$
$$[S\beta_1 \cos \beta_1 (H-z) + b\beta_2 \sin \beta_1 (H-z)], \quad d<z<H \tag{C-19}$$

$$\phi_2 = 2b\, e^{i\omega t} \int_0^\infty J_0(kr)\, kdk\, \frac{\sin \beta_1 d}{V} \cdot$$
$$[S \cos \beta_2 (z-H) - \sin \beta_2 (z-H)], \quad H<z<H+h \tag{C-20}$$

and

$$\phi_3 = 2\, bg\, e^{i\omega t} \int_0^\infty J_0(kr)\, kdk\, \frac{\sin \beta_1 d}{V} \cdot$$
$$[S \cos \beta_2 h - \sin \beta_2 h]\, e^{-i\beta_3 (z-H-h)}, \quad z>H+h \tag{C-21}$$

C-5

Note that Eqs. C-18 and C-19 are identical except for an interchange of the variables z and d.

The solutions of the integrals in Eqs. C-18 thru C-21 may be obtained by evaluation of the appropriate branch cuts in the imaginary k plane and evaluation of the residues. However, in Ref. C-1 it is demonstrated that the results of the integrations in the complex k plane are zero and the normal mode solution is obtained from evaluation of the residues. Therefore, consider the equation for the residues of Eq. C-18, for the upper most layer, which is just:

$$\phi_1' = e^{i\omega t}(-2\pi i) \sum H_o^{(2)}(k_n r) \, k_n \, \frac{\sin \beta_1 z}{\beta_1} \cdot$$

$$\frac{[S \, \beta_1 \cos \beta_1 (H-d) + b\beta_2 \sin \beta_1 (H-d)]}{(\frac{\partial V}{\partial k})_n}$$

(C-22)

C-6

In Eq. C-22, the Bessel function of first order has been replaced
by the Hankel function of the second kind, first order, and the
appropriate summation over the variable k_n. The derivation of the
expression for V represents the evaluation of the residues at
the roots of the equation for V, i.e. $V = 0$. The value of the
derivative is:

$$\frac{\partial V}{\partial k} = \frac{k \; [\quad]}{\beta_1^2 \; \beta_2 \; \cos \; \beta_1 H} \qquad \text{(C-23)}$$

where the factor [ ] is:

$$[\quad] = \left[b(\beta_2^2 - \beta_1^2) \; \sin x \cos x - b\beta_2^2 x - h\beta_1 \cos^2 x \cdot \right.$$
$$(\beta_1^2 + b^2\beta_2^2 \; \tan^2 x) \qquad \text{(C-24)}$$
$$\left. + \frac{ig \; \beta_1 (\beta_3^2 - \beta_2^2) \; \cos^2 x \; (\beta_1^2 + b^2\beta_2^2 \; \tan^2 x)}{\beta_3 \; (\beta_3^2 g^2 - \beta_2^2)} \right]$$

And if Eq. C-17 is solved for S when V is zero, the result
becomes:

$$S = \frac{-b\beta_2 \; \sin \; \beta_1 H}{\beta_1 \; \cos \; \beta_1 H} \qquad \text{(C-25)}$$

Replacing the terms appropriately in Eq. C-22 yields:

C-7

$$\phi_1' = e^{i\omega t}(-2\pi i) \sum H_0^{(2)}(k_n r) \frac{k_n \sin \beta_1 z}{\beta_1 \left[\dfrac{k_n [\ ]_n}{\beta_1^2 \beta_2 \cos \beta_1 H} \right]} \cdot \qquad (C\text{-}26)$$

$$\left[\frac{-b \beta_2 \sin \beta_1 H}{\beta_1 \cos \beta_1 H} \ \beta_1 \cos \beta_1 (H-d) + b \beta_2 \sin \beta_1 (H-d) \right]$$

By straightforward manipulation, the trigonometric terms may be reduced to a more concise set of terms, such that:

$$\phi_1' = -2\pi i \ e^{i\omega t} \sum_n H_0^{(2)}(k_n r) \ \frac{k_n \sin \beta_1 z}{\beta_1} - \frac{b\beta_2 \sin \beta_1 d}{\cos \beta_1 H} \cdot$$

$$\frac{\beta_1^2 \ \beta_2 \cos \beta_1 H}{k_n [\ ]_n} \qquad (C\text{-}27)$$

At this point, it should be noted that the variables z and d are symmetric with each other in Eq. C-27, thereby obviating the need for evaluation of Eq. C-19. Further collection of terms results in:

$$\phi_1 = \frac{2\pi i}{H} b \ e^{i\omega t} \sum_n H_0^{(2)}(k_n r) \ \frac{x_n \ \beta_2^2 \sin (x_n d/H) \sin (x_n z/H)}{[\ ]_n} \qquad (C\text{-}28)$$

For the far field approximation, the Hankel function may be expressed as:

$$H_0^{(2)}(k_n r) \rightarrow \sqrt{\frac{2}{\pi k_n r}} \ e^{i(\pi/4 - k_n r)} \qquad (C\text{-}29)$$

Then the formal solution for the sound velocity potential in the farfield in the upper layer is just:

$$\phi_1 = \frac{2\pi b}{H} \sqrt{\frac{2}{\pi r}} \sum_{n=1}^{\infty} \frac{1}{\sqrt{k_n}} \ e^{i(\omega t - k_n r - \pi/4)} \ \frac{x_n \ \beta_2^{\ 2} \sin\left(\frac{x_n d}{H}\right) \sin\left(\frac{x_n z}{H}\right)}{[\ ]_n}, \ 0 < z < H$$

$$\text{(C-30)}$$

where $[\ ]_n$ is defined by Eq. C-24.

The solution for the middle layer is handled in a similar manner. The residues of Eq. C-20 may be written as:

$$\phi_2 = 2b \ e^{i\omega t} (-2\pi i) \sum_n H_0^{(2)}(k_n r) k_n \ \frac{\sin \beta_1 d}{\left(\frac{\partial V}{\partial k}\right)_n} \ [S \cos \beta_2(z-H) - \sin\beta_2(z-H)]$$

$$\text{(C-31)}$$

As before, the derivative of V with respect to k is evaluated so as to yield the results of Eq. C-23 and C-24. Additionally, as before, the roots of V are determined and the expression for S, Eq. C-25, may be used. The result for the middle layer is then:

$$\phi_2 = -2\pi i \ e^{i\omega t} b \sum_n H_0^{(2)}(k_n r) \ \frac{k_n \sin \beta_1 d}{k_n [\ ]_n} \ \cdot$$

$$\text{(C-32)}$$

$$\frac{\dfrac{\left[-b \ \beta_2 \sin \beta_1 H \cos \beta_2(z-H) - \beta_1 \sin \beta_2(z-H) \cos \beta_1 H\right]}{\beta_1 \cos \beta_1 H}}{\beta_1^{\ 2} \beta_2 \cos \beta_1 H}$$

The trigonometric terms may be simplified somewhat to yield:

$$\phi_2 = \left(\frac{2\pi i b}{H}\right) e^{i\omega t} \sum_n H_0^{(2)}(k_n r) \ \frac{\sin \beta_1 d}{[\ ]_n} \ \cdot$$

$$\text{(C-33)}$$

$$x_n \beta_2 [b\beta_2 \sin x_n \cos\beta_2(z-H) + \beta_1 \cos x_n \sin \beta_2(z-H)]$$

C-9

If the farfield expression for the Hankel function, Eq. C-29 is employed, then the formal solution for the sound velocity potential in the middle layer is:

$$\phi_2 = \left(\frac{2\pi b}{H}\right)\sqrt{\frac{2}{\pi r}} \sum_{n=1}^{\infty} \frac{1}{\sqrt{k_n}} \ e^{i(\omega t - k_n r - \pi/4)} \frac{x_n \beta_2 \ \sin \ (x_n d/H)}{[\ \ ]_n} \cdot \tag{C-34}$$

$$[b \ \beta_2 \ \sin \ x_n \ \cos \ \beta_2 \ (z-H) + \beta_1 \ \cos \ x_n \ \sin \ \beta_2 \ (z-H)], \ H < z < H+h$$

The lower layer may also be evaluated in the same manner as the previous two layers. The residues of Eq. C-21 for the lower layer may be written as:

$$\phi_3 = -2\pi i \ e^{i\omega t} \ bg \sum_n H_0^{(2)}(k_n r) k_n \frac{\sin \ \beta_1 d}{\left(\frac{\partial v}{\partial k}\right)_n} \cdot \tag{C-35}$$

$$(S \ \cos \ \beta_2 h - \sin \ \beta_2 h) \ e^{-i\beta_3(z-H-h)}$$

And again, if the results for Eqs. C-23, C-24 and C-25 are employed, the expression becomes:

$$\phi_3 = -2\pi \ i \ e^{i\omega t} \ bg \sum_n H_0^{(2)}(k_n r) k_n \ \sin \ \beta_1 d \ e^{-i\beta_3(z-H-h)} \cdot$$

$$\frac{\left[\frac{-b \ \beta_2 \ \sin \ \beta_1 \ H}{\beta_1 \ \cos \ \beta_1 \ H} \ \cos \ \beta_2 h - \sin \ \beta_2 h\right]}{\dfrac{k \ [\ \ ]_n}{\beta_1^2 \ \beta_2 \ \cos \ \beta_1 H}} \tag{C-36}$$

If the trigonometric terms of the expression are algebraicly manipulated, the result may be reduced to:

C-10

$$\phi_3 = -2\pi i \, e^{i\omega t} \, bg \sum_n H_0^{(2)} (k_n r) k_n \frac{\sin (\beta_1 d)}{k_n [\ ]_n} \beta_1 \beta_2 \, e^{-i\beta_3(z-H-h)} \ .$$

(C-37)

$$[-b \, \beta_2 \sin \beta_1 H \cos \beta_2 h - \beta_1 \sin \beta_2 h \cos \beta_1 H]$$

And then using the farfield expression for the Hankel function, Eq. C-29, the formal solution for the sound velocity potential in the third layer becomes:

$$\phi_3 = \left(\frac{2\pi b}{H}\right) \sqrt{\frac{2}{\pi r}} \sum_{n=1}^{\infty} \frac{1}{\sqrt{k_n}} \, e^{i(\omega t - k_n r - \pi/4)} \frac{g \, x_n \beta_2 \sin\left(\dfrac{x_n d}{H}\right) e^{-i\beta_3(z-H-h)}}{[\ ]_n} \ .$$

(C-38)

$$[b \, \beta_2 \sin x_n \cos \beta_2 h + \beta_1 \sin \beta_2 h \cos x_n], \ z > H+h$$

The formal solutions for the three layered liquid half space are expressed in Eq. C-30, C-34 and C-38 for the sound velocity potential in the farfield. Two additional procedures can be employed to validate these results. The first is that the value of h can be set to zero, thereby reducing the problem to a two layered liquid case. In this instance, the expressions become the same, and the expression for the third layer becomes equal to the expression for the second layer of the two layer case. The second check is that the expressions for the three layers may be evaluated at each of the two interface boundaries, z=H and z=H+h, to test for continuity. When this is done, the results agree to within the factor "b" of Eq. C-14 for layers one and two and to within the factor "g" of Eq. C-15 for layers two and three, as would be expected.

C-11

DISTRIBUTION LIST

Department of the Navy (Cont'd)   Copies

Office of the Chief of Naval Operations
Attn: Mr. Robert Winokur (OP-095E)
Washington, D.C. 20350   1

Naval Sea Systems Command
Attn: Captain J. W. Organ (NSEA-034)
       Mr. H. F. Murphy (NSEA-031)
Washington, D.C. 20360   1

Naval Electronic Systems Command
Attn: Captain D. B. Murton (PME-124-60)
Washington, D.C. 20360   1

Naval Underwater Systems Center
Attn: Mr. James Gallagher (Code 311)
New London, Connecticut 06320   1

Naval Electronic Systems Command
Attn: Dr. Joel Sinsky (NAVELEX 320)
       Mr. John Cybulski (NAVELEX 320)
Washington, D.C. 20360   1

U.S. Naval Oceanographic Office
Attn: Dr. W. H. Geddes
       Dr. Joji Tomei
NSTL Station, Mississippi 39529   1

Superintendent
U.S. Naval Postgraduate School
Attn: Dr. J. B. Sanders
Monterey, CA 93940   1

Superintendent
U. S. Naval Postgraduate School
Attn: Dr. Ivan Tolstoy and
       Dr. Paul Moose
Monterey, CA 93940   1

Superintendent
U.S. Naval Postgraduate School
Attn: Dr. A. B. Coppens
Monterey, CA 93940   1

Naval Ocean Systems Center
Attn: Dr. John Northrop and
       Dr. Homer Bucker
San Diego, CA 92152   1

Department of the Navy (Cont'd)	Copies

Naval Ocean Systems Center
Attn: Dr. W. K. Lyon (Code 54)
San Diego, CA 92152   1

Naval Ocean Systems Center
Attn: Dr. Edwin Hamilton
San Diego, CA 92152   1

Naval Coastal Systems Center
Attn: Dr. E. Glenn McLeroy (Code 792)
      and Mr. R. Fidler (Code 792)
Panama City, Florida 32401   1

Naval Coastal Systems Center
Attn: Dr. Ken Allen
Panama City, Florida 32401   1

Naval Ocean Research and Development
  Activity
Attn: Dr. Aubrey Anderson (Code 320)
      Mr. Rockne Anderson, Mr. Mike Stanley
      Mr. Stanley Chin-Bing (Code 320), and
      Dr. James Davis (Code 320)
NSTL Station, MS 39529   1

Naval Ocean Research and Development
  Activity
Attn: Dr. Herbert Eppert (Code 360)
      Mr. J. A. Ballard (Code 360)
      Dr. Gerald Morris (Code 340)
NSTL Station, MS 39529   1

Dr. Donald Ross
Deputy Director
SACLANT ASW Research Center
APO, New York 09019   1

Director
Naval Research Laboratory
Attn: Code 8130
4555 Overlook Avenue, S.W.
Washington, D.C. 20375   1

Director
Naval Research Laboratory
Attn: Mr. C. W. Votaw, Code 8123
4555 Overlook Avenue, S.W.
Washington, D.C. 20375   1

Department of the Navy (Cont'd)	Copies

Department of the Navy (Cont'd)   Copies

Director
Naval Research Laboratory
Attn: Mr. O. Diachok (Code 8160)
4555 Overlook Avenue, S.W.
Washington, D.C. 23075   1

Director
Naval Research Laboratory
Attn: Dr. J. A. Bucaro
4555 Overlook Avenue, S.W.
Washington, D.C. 20375   1

Commander
Naval Surface Weapons Center (White Oak)
Attn: WR-41 (Dr. I. Blatstein)
Silver Spring, MD 20910   1

Department of the Air Force

Air Force Office of Scientific
  Research
Attn: Mr. William Best
Building 410, Bolling AFB
Washington, D.C. 20332   1

VELA Seismological Center
Attn: Dr. Robert Rothman and
      Captain M. J. Shore, USAF
312 Montgomery Street
Alexandria, VA 22314   1

Other Government Agencies

U.S. Geological Survey
Attn: Dr. Richard Silwester
Woods Hole, MA 02543   1

The National Science Foundation
Attn: Dr. Roy Hanson and
      Dr. Don Heinrichs
Washington, D.C. 20550   1

Commercial Agencies	Copies
The Pennsylvania State University Applied Research Laboratory Attn: Mr. Nick Abourezk P. O. Box 30 State College, PA 16801	1
Scripps Institution of Oceanography/ Marine Physics Laboratory Attn: Dr. George Shor University of California La Jolla, CA 92037	1
Professor Gunter Ziehm Forfchungs-Anstalt Der Bunderwehr Fur Wasfere Chall-Und Geophysik Klaus Dorfer Weg 2-24 D-2300 Kiel 14 Federal Republic of Germany	1
The Applied Physics Laboratory Attn: Dr. James A. Mercer 1013 North East 40th HN-10 Seattle, Washington 98195	1
The Courant Institute of Mathematical Sciences Attn: Dr. David Stickler New York University 251 Mercer Street New York, NY 10012	1
Department of Geological Sciences Attn: Dr. Jack Oliver and Dr. Bryan Isacks McGraw Hall Cornell University Ithaca, NY 14850	1

The Lamont-Doherty Geological
  Observatory of Columbia University
Attn: Mr. Robert E. Houtz and
        Dr. Robert Stoll
Palisades, NY 10964
	1

The Johns Hopkins University Applied Physics Laboratory Attn: Mr. Gene Byron Johns Hopkins Road Laurel, MD 20810	1

Commercial Agencies (Cont'd)   Copies

Woods Hole Oceanographic Institution
Attn: Dr. John Ewing and
        Dr. Earl Hayes
Woods Hole, MA   02543   1

The Applied Research Laboratories of
   The University of Texas at Austin
Attn: Dr. Lloyd Hampton and
        Dr. Ken Hawker
P. O. Box 8029
Austin, TX   78712   1

Hawaii Institute of Geophysics
Attn: Dr. George Sutton and
        Dr. Dan Walker
University of Hawaii
2525 Correa Rd.
Honolulu, Hawaii   96822   1

The University of Washington
Attn: Dr. Rubens Sigelmann
Electrical Engineering Dept.
Seattle, Washington   98195   1

The Marine Science Institute
   of the University of Texas
Attn: Dr. Joseph Worzel and
        Dr. Gary Latham
P. O. Box 7999
University Station
Galveston, TX   77550   1

The Marine Science Institute
   of the University of Texas
Attn: Dr. H. James Dorman
P. O. Box 7999
University Station
Galveston, TX   77550   1

The Marine Science Institute
   of the University of Texas
Attn: Dr. Mark Houtz
P. O. Box 7999
University Station
Galveston, TX   77550   1

Commercial Agencies (Cont'd)   Copies

Planning Systems, Inc.
Attn: Dr. Louis P. Solomon
7900 Westpark Dr.
McLean, VA 22101   1

Polar Research Laboratory
Attn: B. Buck
123 Santa Barbara Street
Santa Barbara, CA 93101   1

Tracor, Inc.
Attn: Mr. Robert Urick
1601 Research Boulevard
Rockville, MD 20850   1

Underwater Systems, Inc.
Attn: Mr. Richard Hecht
8121 Georgia Avenue
Silver Spring, MD 20910   5

Underwater Systems, Inc.
Attn: Mr. Dan Woolston
8121 Georgia Avenue
Silver Spring, MD 20910   5

The Weston Geophysical Corporation
Attn: Mr. Andrew LeCroix
P. O. Box 550
Westborough, MA 01581   1

Dr. F. L. Dowling
R.R. 3, Box 123
Westby, WI   1

The Institute of Acoustic Research
Attn: Dr. Morton Kronengold and
       Dr. Don Fletcher
615 SW 2nd Avenue
Miami, FL 33130   1

Boeing Aerospace Company
Attn: Mr. Bob Arnold
Tactical Systems Concepts
Advanced Projects
P.O. Box 3999, M.S. 84-63
Seattle, Washington 98124   1

Commercial Agencies (Cont'd)	Copies
MIT, Lincoln Laboratories Attn: Dr. Thomas Landers and Dr. Richard Lacoss 42 Carleton Street Cambridge, MA 02142	1
Mr. Ian Sargent 801 North Fairway Road Northwoods Glenside, PA 19038	1
ENSCO, Inc. Attn: Mr. James Caldwell 5408A Port Royal Road P. O. Box 1346 Springfield, VA 22151	1